Title
Changes in nitrogen oxides emissions in California during 2005–2010 indicated from top-down and bottom-up emission estimates

Journal
Journal of Geophysical Research: Atmospheres, 119(22)

ISSN
2169-897X

Authors
Huang, Min
Bowman, Kevin W
Carmichael, Gregory R
et al.

Publication Date
2014-11-27

DOI
10.1002/2014jd022268

AGU PUBLICATIONS

JGR

Journal of Geophysical Research: Atmospheres

RESEARCH ARTICLE
10.1002/2014JD022268

Key Points:
- OMI and surface NO_2 are assimilated separately/jointly using 4D-Var method
- Our top-down estimates are consistent with the latest CARB bottom-up inventory
- Uncertainties in modeled surface O_3 in the Western U.S. are overall reduced

Supporting Information:
- Readme
- Section S1
- Figure S1
- Figure S2
- Figure S3
- Figure S4

Correspondence to:
M. Huang,
min.huang@jpl.nasa.gov

Citation:
Huang, M., et al. (2014), Changes in nitrogen oxides emissions in California during 2005–2010 indicated from top-down and bottom-up emission estimates, *J. Geophys. Res. Atmos.*, *119*, 12,928–12,952, doi:10.1002/2014JD022268.

Received 2 JUL 2014
Accepted 17 OCT 2014
Accepted article online 23 OCT 2014
Published online 21 NOV 2014

Changes in nitrogen oxides emissions in California during 2005–2010 indicated from top-down and bottom-up emission estimates

Min Huang[1], Kevin W. Bowman[1], Gregory R. Carmichael[2], Tianfeng Chai[3], R. Bradley Pierce[4], John R. Worden[1], Ming Luo[1], Ilana B. Pollack[5,6], Thomas B. Ryerson[6], John B. Nowak[5,6,7], J. Andrew Neuman[5,6], James M. Roberts[6], Elliot L. Atlas[8], and Donald R. Blake[9]

[1]Jet Propulsion Laboratory, California Institute of Technology, Pasadena, California, USA, [2]Center for Global and Regional Environmental Research, University of Iowa, Iowa City, Iowa, USA, [3]NOAA Air Resources Laboratory, College Park, Maryland, USA, [4]NOAA National Environmental Satellite, Data, and Information Services, Madison, Wisconsin, USA, [5]Cooperative Institute for Research in Environmental Sciences, University of Colorado Boulder, Boulder, Colorado, USA, [6]NOAA Earth System Research Laboratory, Boulder, Colorado, USA, [7]Now at Aerodyne Research Inc., Billerica, Massachusetts, USA, [8]Department of Atmospheric Sciences, University of Miami, Miami, Florida, USA, [9]Department of Chemistry, University of California, Irvine, California, USA

Abstract In California, emission control strategies have been implemented to reduce air pollutants. Here we estimate the changes in nitrogen oxides ($NO_x = NO + NO_2$) emissions in 2005–2010 using a state-of-the-art four-dimensional variational approach. We separately and jointly assimilate surface NO_2 concentrations and tropospheric NO_2 columns observed by Ozone Monitoring Instrument (OMI) into the regional-scale Sulfur Transport and dEposition Model (STEM) chemical transport model on a $12 \times 12\ km^2$ horizontal resolution grid in May 2010. The assimilation generates grid-scale top-down emission estimates, and the updated chemistry fields are evaluated with independent aircraft measurements during the NOAA California Nexus (CalNex) field experiment. The emission estimates constrained only by NO_2 columns, only by surface NO_2, and by both indicate statewide reductions of 26%, 29%, and 30% from ~0.3 Tg N/yr in the base year of 2005, respectively. The spatial distributions of the emission changes differ in these cases, which can be attributed to many factors including the differences in the observation sampling strategies and their uncertainties, as well as those in the sensitivities of column and surface NO_2 with respect to NO_x emissions. The updates in California's NO_x emissions reduced the mean error in modeled surface ozone in the Western U.S., even though the uncertainties in some urban areas increased due to their NO_x-saturated chemical regime. The statewide reductions in NO_x emissions indicated from our observationally constrained emission estimates are also reflected in several independently developed inventories: ~30% in the California Air Resources Board bottom-up inventory, ~4% in the 2008 National Emission Inventory, and ~20% in the annual mean top-down estimates by Lamsal et al. using the global Goddard Earth Observing System (GEOS)-Chem model and OMI NO_2 columns. Despite the grid-scale differences among all top-down and bottom-up inventories, they all indicate stronger emission reductions in the urban regions. This study shows the potential of using space-/ground-based monitoring data and advanced data assimilation approach to timely and independently update NO_x emission estimates on a monthly scale and at a fine grid resolution. The well-evaluated results here suggest that these approaches can be applied more broadly.

1. Introduction

Nitrogen dioxide (NO_2) is one of the six criteria air pollutants regulated by U.S. Environmental Protection Agency (EPA) since the 1970s (http://www.epa.gov/air/nitrogenoxides), as both short- and long-term exposures to NO_2 are harmful for human respiratory system [*U.S. Environmental Protection Agency* (*EPA*), 2013]. The primary National Ambient Air Quality Standards (NAAQS) that aim at protecting human health are currently set at 100 ppbv for the 3 year averaged 98th percentile of hourly NO_2 and at 53 ppbv for the annual mean NO_2. In addition to its own impacts on human health, NO_2 is one of a group of highly reactive gaseous nitrogen oxides ($NO_x = NO + NO_2$) that affects tropospheric chemistry and contributes to near-surface ozone (O_3) and particulate matter (PM) pollution. Ozone and PM also belong to the EPA-regulated six criteria air pollutants, and the levels of their NAAQS tend to become more stringent in the future. For example, EPA proposed to lower the

national primary O_3 standard to a level within 60–70 ppbv [*U.S. EPA*, 2010]. Extended regions in the U.S. are projected to violate the proposed standard, and higher costs for reducing the O_3 levels are expected in response to the potential new thresholds [*McCarthy*, 2010]. Therefore, it is important to understand NO_x concentrations and their temporal changes, the major factors affecting these changes (e.g., local and regional emissions), and how these impact the distributions of secondary pollutants such as O_3.

California is the most populous and the third largest state in the U.S. [*U.S. Census Bureau 2010*, 2011] and has diverse topography, climate, and emission sources of air pollutants. The entire state has complied with the NAAQS NO_2 standards [*California Air Resources Board* (*CARB*), 2014]. Various types of observations generally show significant reductions in NO_x over California during the past decades. A decreasing trend of ~3% yr^{-1} is found based on surface in situ NO_x measurements from multiple monitoring networks, which are denser at populated regions and/or near the major emission source regions (http://www.epa.gov/airtrends/nitrogen.html) [*Pollack et al*., 2013, and references therein]. Satellites routinely measure NO_2 as a whole column at certain time(s) of a day with broad geographic coverage, and these NO_2 columns over California reflect faster decreasing rates during 2005–2010 than those based on the surface observations, i.e., on average, $>$4% yr^{-1} statewide and $>$10% yr^{-1} over some urban regions [*Russell et al*., 2010, 2012]. The differences in NO_2 trends determined by surface in situ and satellite measurements can be attributed to the varied measurement uncertainties and sampling (spatial and temporal) strategies, as well as the complex relationships between surface and column NO_2.

The observed NO_x in California is largely affected by local and regional NO_x emissions. A majority ($>$80%) of California's NO_x emissions come from mobile sources, mainly over the populated regions such as South Coast, Bay Area, and the Central Valley [*CARB*, 2014; *McDonald et al*., 2012]. The decreasing trends in observed NO_2 over California are largely due to the reductions in its anthropogenic NO_x emissions by effectively switching the fuel types and the implementation of combustion control. Timely updating the NO_x emission estimates to account for its temporal changes can help better interpret the distributions, trends, and variability of the observed NO_x.

Based on the existing emission estimates for a historical year, emissions for a later year can be derived using two typical methods to reflect the temporal changes: (1) projecting bottom-up emission estimates from a historical year to a future year, using the information of population and economic growth and the implemented emission control measures between these two years, and (2) applying top-down approaches by integrating observations, and usually, transport models are involved. Using the bottom-up method, California Air Resources Board (CARB) estimated a 28% reduction in anthropogenic NO_x emissions from 2005 to 2010 [*CARB*, 2014], above the nationwide changes of ~25% provided by *Xing et al*. [2013] and U.S. EPA (http://www.epa.gov/ttnchie1/trends). These types of inventories are generally updated more frequently in California than in many developing countries where the pollution levels are high in magnitude and variability and the information for accurately projecting emissions is lacking. The top-down emission estimates may be generated faster than the bottom-up inventories, but their accuracy depends on model parameterizations and configurations, the characteristics of observations incorporated, and the methods used. Following the method described in *Lamsal et al*. [2011], the same group of researchers at Dalhousie University produced grid-specific annual mean NO_x emission scaling factors from 2005 to 2010 using the global Goddard Earth Observing System(GEOS)-Chem chemical transport model and Ozone Monitoring Instrument (OMI) NO_2 columns. This product indicates a ~20% decrease in California's anthropogenic NO_x emissions during this period (Figure S1 in the supporting information, adapted from http://fizz.phys.dal.ca/~atmos/martin/?page_id=123). In another study, using a combined Weather Research and Forecasting (WRF) (Eulerian)–FLEXible PARTicle dispersion (Lagrangian) modeling system and aircraft observations in May–June 2010, *Brioude et al*. [2013] lowered the total reactive nitrogen (NO_y) emissions from the 2005 National Emission Inventory (NEI 05) by 32% and 27% in California's Los Angeles (LA) County and South Coast Air Basin, respectively. Updating NO_x emissions on regional scales over the entire state using ground-/space-based air monitoring data and advanced assimilation methods that account for the life cycle of chemical species has not been covered in existing studies but is needed. The effects of used models, observations, and methods on the assimilation results also need to be carefully analyzed and discussed. A better understanding of current capabilities and limitations of top-down techniques will timely improve emission estimates and model predictability and also assist the evaluation of implemented emission control strategies and bottom-up emission projection methodology.

Although O_3 and its precursor species (NO_x, carbon monoxide (CO), and volatile organic compounds (VOCs)) over many Californian areas showed decreasing trends in the past few decades based on various types of measurements [e.g., *CARB*, 2014; *Pollack et al*., 2013; *Russell et al*., 2012; *Warneke et al*., 2012; *Brioude et al*., 2013; *Pusede and Cohen*, 2012, and the references therein], a number of air basins/districts still violate the current and projected O_3 standards, most of which are located in the South Coast and San Joaquin Valley [*Huang et al*., 2013; http://www.arb.ca.gov/adam/select8/sc8start.php; *U.S. EPA*, 2014]. Previous studies found that emissions in California in spring and summer can affect air quality in downwind areas as far as thousands of kilometers away, causing O_3 exceedances over a broad region in the Western U.S. [*Tong and Mauzerall*, 2008; *Langford et al*., 2010; *Huang et al*., 2013; *Burley et al*., 2014; *VanCuren*, 2014]. Therefore, it is also important to assess the impacts of NO_x emission changes in California on the distributions of secondary pollutants in California and its downwind states in the Western U.S.

In May 2010, a major multi-institution field campaign was coordinated by the National Oceanic and Atmospheric Administration (NOAA), entitled California Nexus (CalNex): Research at the Nexus of Air Quality and Climate Change. This field experiment provided measurements of various trace gases and aerosols in California using a suite of measurement platforms, and assessing emission inventories is one of its major research objectives [*Ryerson et al*., 2013]. In this paper, we use the full-chemistry version of the regional-scale Sulfur Transport and dEposition Model (STEM) and its adjoint model at $12 \times 12\ km^2$ horizontal resolution to assess the changes in NO_x emissions during 2005–2010 over California and the impacts on O_3 in the Western U.S. during this month. Specifically, we characterize the uncertainties in bottom-up emission estimates that have different base years in terms of statewide total emissions and their spatial variability. We also update a selected bottom-up emission inventory via the assimilation of surface and satellite NO_2 observations separately and jointly using the four-dimensional variational (4D-Var) approach and evaluate the updated chemistry fields using the nonassimilated observations (i.e., aircraft measurements during CalNex and O_3 at surface monitoring sites).

This paper first introduces the observational data used, the STEM model configurations, and the 4D-Var method (section 2). In section 3.1, we evaluate the model a priori with surface, aircraft, and satellite measurements. We then show the a posteriori NO_x emission estimates, evaluate the updated NO_2 and O_3 distributions, and discuss the NO_x emission trends during 2005–2010 indicated by multiple emission data sets (section 3.2). Finally, the summary and suggested future work are presented in section 4.

2. Methods and Data Sets

2.1. Observations and Their Uncertainties

2.1.1. Tropospheric NO_2 Column Measurements From OMI

OMI is a nadir-viewing charge-coupled device spectrometer on board the NASA Aura satellite launched in 2004. OMI has an across-track swath of 2600 km, subdivided into 60 across-track pixels, which provides daily global coverage with ground pixel sizes of $13 \times 24\ km^2$ at nadir and significantly larger at the edges of the swath. Covering 270–500 nm (in the ultraviolet (UV) and visible (vis) ranges) on the spectra, OMI measures a few key chemical species including NO_2 during the daytime (at local time ~1:40 P.M.) for air quality studies on urban, regional, and global scales [*Russell et al*., 2010, 2011, 2012; *Lamsal et al*., 2008, 2011, 2013; *Beirle et al*., 2011; *Witte et al*., 2011; *Duncan et al*., 2010, 2014; *Valin et al*., 2013, 2014; *Bechle et al*., 2013; *Herron-Thorpe et al*., 2010]. Some of these studies have demonstrated the advantages of OMI's finer spatial resolution over the measurements from several other satellite instruments; e.g., *McLinden et al*. [2012] showed that OMI presents similar NO_2 spatial distributions over the Canadian oil sands with Scanning Imaging Absorption Spectrometer for Atmospheric Chartography (SCIAMACHY), Global Ozone Monitoring Experiment (GOME), and GOME2 but in greater detail.

The OMI tropospheric NO_2 vertical columns are retrieved in three steps: (1) determine a slant column density from a spectral fit to the Earth reflectance spectrum with the differential absorption spectroscopy (DOAS) approach, (2) quantify the stratospheric contribution to the slant column, and (3) apply air mass factor (AMF) to convert the residual tropospheric slant column to the tropospheric column [*Boersma et al*., 2007, 2011a]. The AMFs depend on the viewing geometry, the atmospheric scattering (computed by a radiative transfer model), and the vertical distribution of NO_2 (i.e., the shape factor, or NO_2 a priori profile, based on chemical transport model calculations or some prior knowledge) [*Palmer et al*., 2001]. There are three tropospheric

column NO_2 products independently generated by the Royal Netherlands Meteorological Institute (KNMI), NASA, and UC Berkeley. All of the three retrieval products use the same DOAS technique to determine the slant column described in step (1). The KNMI and NASA algorithms differ in the above retrieval steps (2) and (3). The Berkeley group uses the NASA method to subtract stratospheric contribution (step (2)), but modifies its step (3) to determine the AMFs [*Russell et al*., 2011]. Notable differences have been found among the various OMI NO_2 products due to a number of factors such as surface albedo, terrain, and the NO_2 a priori profiles used in the retrieval [e.g., *Russell et al*., 2011; *Heckel et al*., 2011; *Boersma et al*., 2011b].

In this study, we use the destriped KNMI OMI NO_2 column product in May 2010, the version 2.0, for model evaluation and assimilation (Table 1). *Miyazaki et al*. [2012a, 2012b] find that the biases in the satellite retrievals used in data assimilation can affect the emission a posteriori. Our choice from multiple versions of OMI products is primarily based on previous analysis on their data quality in spring and summer [e.g., *Lamsal et al*., 2010; *Boersma et al*., 2008, 2009, 2011b]. As successful assimilation studies require accurate observation operators, an additional reason we use the KNMI product is that it explicitly provides averaging kernel vectors [*Eskes and Boersma*, 2003], which will be described in detail in the following paragraphs. Careful validation of each OMI product with in situ measurements during the studied period and region can be valuable but is beyond the scope of this study. Due to the lack of such information, no bias correction was applied on the assimilated OMI columns. As the biases in OMI product can be spatially variable, taking the suggestions by *Heckel et al*. [2011], discussions on the assimilation results on large spatial scales can reduce the influences of omitting the bias correction. Cross validation with independent observations and emission inventories will be performed to directly indicate the effectiveness of assimilation.

Following the recommendations in the Users' Guide [*Boersma et al*., 2011a] and recent studies [*Duncan et al*., 2014; *Pfister et al*., 2013], we select the KNMI OMI data based on tropospheric column flag (=0, which also excluded the unreliable pixels affected by the row anomaly that occurred since 2007), surface albedo (<0.3), cloud radiance fraction (<0.3), solar zenith angle ($<75°$), viewing zenith angle ($<45°$), and the instrument detection limit ($>1.0\times10^{15}$ molecule/cm^2, same as in *Lamsal et al*. [2011]). The averaging kernels (AKs) **A** [*Eskes and Boersma*, 2003] and AMFs in the KNMI product were used to calculate the modeled tropospheric NO_2 vertical columns y_{trop} comparable to OMI's by mapping the modeled $\mathbf{x_{trop}}$ vectors of NO_2 subcolumns via the AKs, based on equations (1) and (2) below, which were adapted from equations (6) and (5) in *Boersma et al*. [2011a].

$$\mathbf{A_{trop}} = \mathbf{A} \cdot \mathrm{AMF_{total}}/\mathrm{AMF_{trop}} \quad (1)$$

$$y_{trop} = \mathbf{A_{trop}} \cdot \mathbf{x_{trop}} \quad (2)$$

where $\mathbf{x_{trop}}$ refers to the vector of the NO_2 subcolumns in the STEM model vertical layers in the troposphere. The AK vectors indicate the relative sensitivity of an instrument to the measured species within the vertical layers throughout the column, and OMI shows lower sensitivity to NO_2 near the surface (i.e., the values in **A** are mostly <1.0 at these altitudes) than in the free troposphere (with the values in **A** mostly >1.0). Computed from AMFs, **A** depends on many factors such as NO_2 a priori profiles, surface albedo, and the presence of clouds and aerosols [*Eskes and Boersma*, 2003]. Figure S2 demonstrates the impact of surface albedo on the shape of **A** in California on a specific day. The **A** vectors in the KNMI product are specified at the Tropospheric Model 4 (TM4) grid used in their retrieval. In our calculations of y_{trop}, the **A** vectors were interpolated to the finer STEM model pressure levels using a univariate interpolation approach [*Akima*, 1970]. This interpolation is suggested in principle, but when the averaging kernel vectors are sensitive to changes on small spatial scales, such as due to rapid cloud changes, the interpolation is discouraged [*Boersma et al*., 2011a]. However, in our case, OMI data measured under cloudy conditions were excluded from the analysis. The usage of **A** here is designed to remove the measurement errors contributed from the TM4 a priori profiles.

2.1.2. Surface NO_2 Measurements and Bias Correction

Hourly NO_2 measurements in May 2010 from the Air Quality and Meteorological Information System (AQMIS2, Table 1), maintained by CARB at a number of surface sites were also used for model evaluation and assimilation. Most of the surface NO_2 measurements taken by chemiluminescence (CL) detection with catalytic conversion on a molybdenum surface are known to be sensitive to some other NO_y species, most strongly to alkyl nitrates (AN), peroxyacetyl nitrates (PAN), and nitric acid (HNO_3). Therefore, they can have variable positive biases [*Winer et al*., 1974; *Dunlea et al*., 2007; *Steinbacher et al*., 2007]. We applied bias correction factors (CFs) on the original measurements before using them for quantitative analysis. These CFs

Journal of Geophysical Research: Atmospheres

10.1002/2014JD022268

Table 1. Observations Used in This Study[a]

Network or Platform	Measurement	Technique	References of Instrument Details and Data Quality	Data Source	Purpose in This Study
OMI	Daily tropospheric NO_2 column, KNMI v2.0	Retrieved from UV-vis backscattered radiation	*Boersma et al.* [2007, 2011a]	http://www.temis.nl/airpollution/no2.html	Assimilation; model evaluation
CARB/AQMIS	Hourly surface NO_2	CL detection with catalytic conversion on a molybdenum surface	NA	http://www.arb.ca.gov/aqmis2/aqmis2.php	Assimilation; model evaluation
NOAA WP-3D aircraft <2 km agl	NO_2	CL detection with UV-LED photolytic conversion	*Pollack et al.* [2011]	http://esrl.noaa.gov/csd/groups/csd7/measurements/2010calnex/P3/DataDownload	Model evaluation
	O_3	CL	*Ryerson et al.* [1998]		
	PAN	Thermal decomposition–Chemical Ionization Mass Spectrometry using I^- reagent	*Roiger et al.* [2011]		
	HNO_3	Chemical Ionization Mass Spectrometry using SiF_5^- reagent	*Neuman et al.* [2002]		
	ANs (C1-C5)	Advanced Whole Air Sampler	*Colman et al.* [2011]; https://www.eol.ucar.edu/content/documentation-2		
AQS	Hourly O_3	UV absorbance	*Office of Air Quality Planning and Standards* [*2008*] *and Zhang et al.* [2012]	http://www.epa.gov/ttn/airs/airsaqs/detaildata	Model evaluation
CASTNET	Hourly O_3	UV absorbance	*CASTNET* [2011]	http://epa.gov/castnet/javaweb/index.html	Model evaluation
OMI	Daily total O_3 columns	Retrieved from UV backscattered radiation	*Levelt et al.* [2006] and *McPeters et al.* [2008]	ftp://toms.gsfc.nasa.gov/pub/omi/data/ozone/Y2010/	Assimilation in boundary condition model RAQMS; an input of STEM model
TES	Daily (at both daytime and nighttime) O_3 profiles	Retrieved from high spectral resolution thermal radiances	*Beer* [2006], *Bowman et al.* [2006], *Nassar et al.* [2008], *Richards et al.* [2008], *Boxe et al.* [2010], and *Verstraeten et al.* [2013]	http://tes.jpl.nasa.gov/data/	Model evaluation

[a]See text for definitions of acronyms.

were calculated based on the STEM model a priori (defined in section 2.2) chemical fields at the corresponding grids of the surface sites, following equation (3) as suggested by *Lamsal et al*. [2008]:

$$\mathrm{CF\ (unitless)} = [\mathrm{NO_2}]/([\mathrm{NO_2}] + \Sigma[\mathrm{AN}] + 0.95[\mathrm{PAN}] + 0.35[\mathrm{HNO_3}]) \quad (3)$$

Similar bias correction methods have been used in other inverse modeling studies in the U.S. [e.g., *Tang et al*., 2013]. We are aware that this bias correction approach has two major limitations:

1. Equation (3) was derived based on findings in multiple laboratory and field experiment studies. It focused on the OMI overpass times, and the conversion efficiency for HNO_3 may be highly uncertain [*Neuman et al*., 1999; *Lamsal et al*., 2008, 2010]. Therefore, there exist limitations to correct the biases in surface NO_2 measurements at all locations and times using this same equation.
2. The model-based CFs can introduce uncertainties. To examine how well this CF metric is represented by the model, the modeled CF fields are compared in section 3.1.2 against those calculated from the aircraft observations.

We also conducted assimilation of surface nitrogen monoxide (NO) measurements at California surface sites. Although these measurements are not interfered by non-NO_2 species, at many of these surface sites the measured NO are of much poorer arithmetic precision than the measured NO_2, and they can be more strongly affected by local sources and therefore are not suitable for this study.

Compared to the column amounts that are sensitive to fluxes from various origins and therefore are affected by synoptic to local-scale meteorology, surface concentrations may be more sensitive to the near-surface dynamics, which is usually challenging to model accurately, especially at the nighttime. The impacts of transport errors on the assimilation of column or surface measurements will need to be carefully evaluated by conducting additional analysis using multimodel framework and single-model ensemble methods (e.g., a large number of meteorological model simulations using different configurations) [*Lauvaux and Davis*, 2014, and the references therein], and using the subsets of the available observations.

2.1.3. Aircraft Observations

We use the near-surface (below 2 km, above ground level (agl)) O_3 and NO_2 observations collected during multiple NOAA WP-3D flights over California in May 2010 to assess the effectiveness of the assimilation of surface and column NO_2 observations (Table 1). These data were not assimilated and were saved to evaluate the modeled chemistry fields. We also use the aircraft ANs, PAN, and HNO_3 measurements to evaluate the modeled CF fields. The NO_2, O_3, HNO_3, PAN, and ANs (C1–C5) were measured by CL detection with photolytic conversion (which is almost nonsensitive to non-NO_2 species) [*Pollack et al*., 2011], CL [*Ryerson et al*., 1998], Chemical Ionization Mass Spectrometry [*Neuman et al*., 2002], thermal decomposition–Chemical Ionization Mass Spectrometry [*Roiger et al*., 2011], and Advanced Whole Air Sampler [*Colman et al*., 2011] (https://www.eol.ucar.edu/content/documentation-2), with uncertainties (accuracy/precision) in their original resolutions of 4%/(0.03–0.08) ppbv, 2%/(0.015–0.15) ppbv, 15%/0.012 ppbv, 20%/0.005 ppbv, and 10%/2%, respectively. Most of these measurements in this month were taken over Southern California (SoCal). The 1 min merged data were used to evaluate the modeled NO_2 and O_3 in the following sections. Observations in this merged data set have a closer spatial resolution (WP-3D aircraft has a top speed of ~12.4 km/min) to STEM's. The observation-based CFs were calculated using another merged data set in the resolution of the Advanced Whole Air Sampler.

2.1.4. Other O_3 Measurements

Hourly O_3 from U.S. EPA Air Quality System (AQS) and Clean Air Status and Trends Network (CASTNET) sites in May 2010 are used to evaluate the modeled surface O_3 in multiple STEM simulations. The AQS and CASTNET O_3 were measured by the UV absorbance method, with accuracy of ±2% and ±10%, respectively [*Office of Air Quality Planning and Standards*, 2008; *Zhang et al*., 2012; *CASTNET*, 2011]. Daily OMI total O_3 columns, also assimilated into the boundary condition model (details in section 2.2), were used in the online Tropospheric Ultra-violet Visible (TUV) radiation model [*Madronich et al*., 2002] to generate the photolysis rates for STEM. OMI total O_3 column are shown to be ~0.4% higher than ground-based network of Dobson and Brewer instruments [*McPeters et al*., 2008]. We also used Level 2 (L2) O_3 profiles measured during both daytime and nighttime from the Tropospheric Emission Spectrometer (TES) instrument [*Beer*, 2006] on board the Aura satellite to assess the modeled O_3 vertical distributions in the Western U.S. Details of TES O_3 are introduced in section S1.

Table 2. Monthly Long Simulations Conducted in This Study[a]

Cases	Assimilated Observations	Emission Inputs (Short Forms and the Full Descriptions)	Domain
F_{SNEI05}	/	E_{SNEI05}: anthropogenic sectors from scaled NEI 05	Western U.S.[b]
$F_{CARB10v13}$	/	$E_{CARB10v13}$: CARB inventory for year 2010, projected from base year of 2008 (released in March 2013), including all sectors	Western U.S.
F_{NEI08}	/	E_{NEI08}: anthropogenic sectors from NEI 08 (from Harvard University where the NEI 08 inputs for the standard GEOS-Chem simulations were created from the same source emission files developed by U.S. EPA)	Western U.S.
F_{SNEI05_ACOL}	/	E_{ACOL} in California grid boxes from the A_{COL} case; E_{SNEI05} in the rest of the model grid boxes	Western U.S.
F_{SNEI05_ASUR}	/	E_{ASUR} in California grid boxes from the A_{SUR} case; E_{SNEI05} in the rest of the model grid boxes	Western U.S.
A_{COL}	KNMI OMI tropospheric NO_2 columns	a priori: E_{SNEI05} a posteriori: E_{ACOL}	California[c]
A_{SUR}	surface NO_2 volume mixing ratios corrected by model-based CFs	a priori: E_{SNEI05} a posteriori: E_{ASUR}	California
A_{BOTH}	Both column and surface NO_2	a priori: E_{SNEI05} a posteriori: E_{ABOTH}	California

[a]In the Case Names, "F" Represents Forward Simulations, "A" Represents Assimilation, and "E" Represents Emission Estimates.
[b]Latitude/longitude ranges for this domain defined in section 2.2.
[c]Latitude/longitude ranges for this domain defined in section 2.3.

2.2. Model and Its Configurations

The model simulations were conducted using the full-chemistry version of the STEM model on a $12 \times 12\ km^2$ Lambert conformal conic grid with 32 vertical layers in the troposphere over the Western U.S. (180×150 grid boxes, approximate latitude/longitude ranges: 30–48°N/130–100°W). The model calculates gas-phase chemistry reactions based on the Statewide Air Pollution Research Center (SAPRC) gaseous chemical mechanism (SAPRC-99) [*Carter*, 2000] with 30 photolysis rates calculated online by the TUV radiation model. STEM has been used and evaluated in a number of field campaigns in the past decade [*Carmichael et al*., 2003a, 2003b; *Tang et al*., 2007, 2004; *Stith et al*., 2009; *Adhikary et al*., 2010; *Huang et al*., 2010, 2011]. STEM simulations were conducted on 60 km and 12 km horizontal resolution grids for CalNex period, and the O_3 fields have been carefully compared with various observations and other chemical transport models [*Huang et al*., 2013; *Lapina et al*., 2014].

The STEM calculations were driven by meteorological fields generated by the Advanced Research Weather Research and Forecasting Model (WRF-ARW) version 3.3.1 [*Skamarock et al*., 2008]. *Huang et al*. [2013] overviewed the meteorological conditions in May 2010 and described in detail the WRF configurations and the comparison of the simulated meteorological fields with aircraft observations.

The lateral boundary conditions for gaseous and aerosol species and top boundary conditions for 10 gaseous species were downscaled from the archived ($1° \times 1°$ horizontal and 6-hourly temporal resolution) Real-time Air Quality Modeling System (RAQMS) global real-time chemical analyses [*Pierce et al*., 2007] which assimilated the OMI O_3 columns and the Microwave Limb Sounder instrument (also on board the Aura satellite) stratospheric O_3 profiles. The assimilated RAQMS O_3 profiles show fairly good agreement ($<\pm 20\%$ mean biases) with in situ measurements and ozonesondes in California [*Pierce et al*., 2011], which can also be reflected in our comparison of STEM O_3 against the TES L2 O_3 profiles (section 3.2.4). Indicated from the comparison between STEM-modeled NO_x and aircraft NO_x measurements in May 2010, the vertical structure of NO_x is also generally captured ($<\pm 10\%$ biases for the median profiles) by RAQMS above ~2 km with an underpredicted variability [*Huang et al*., 2013].

The bottom-up emission inventory used as the a priori in the assimilation in this study was the same set as those in *Huang et al*. [2013], defined here as E_{SNEI05} (Table 2): The anthropogenic emissions came from NEI 05 (E_{NEI05}, ftp://aftp.fsl.noaa.gov/divisions/taq/emissions_data_2005), which varies on weekdays and weekends

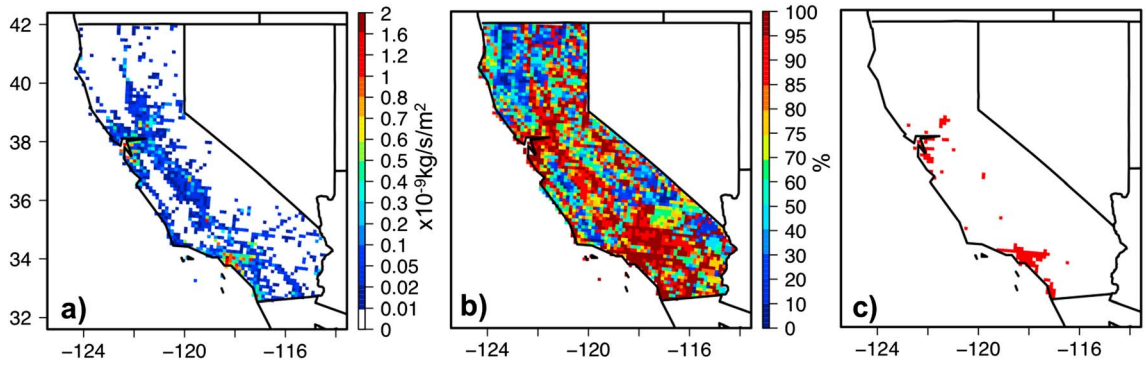

Figure 1. (a) Monthly-mean a priori NO_x ($NO + NO_2$) emission estimates (i.e., E_{SNEI05} in Tables 2 and 4) used in the assimilation, including sources from all sectors. (b) The contributions of the anthropogenic sources to the total NO_x emissions shown in Figure 1a. (c) The urban regions (filled in red) defined in our WRF simulation, based on the IGBP-modified MODIS land use classification, which shows expanded urban areas in California than what the WRF-default U.S. Geological Survey classification indicates (see details in *Huang et al.* [2013]).

and includes diurnal cycles. We assume that this inventory represents the anthropogenic emissions in the base year of 2005, in which California NO_x emissions (~0.3 Tg N/yr) contribute to ~5% of the national NO_x emissions. The emissions for CO, NO_x, and VOCs were scaled by −25%, −20%, and −15%, respectively, primarily based on the information from the U.S. EPA emission trends during 2005–2010 (http://www.epa.gov/ttnchie1/trends) but also accounted for the NO_x emission trends in California indicated from the emission scaling factor product by Lamsal et al. (Figure S1). The a posteriori emission estimates shown in section 3.2 will be compared to the original NEI 05 to indicate the NO_x emission trends during 2005–2010. Anthropogenic NO_x emissions contribute to >95% of the statewide NO_x emissions in this inventory (Figure 1b). About half of these emissions in California were contributed by sources in the urban areas that cover only <5% of the entire state (Figure 1c); the definition of urban areas in this study is based upon the International Geosphere-Biosphere Programme (IGBP)-modified Moderate Resolution Imaging Spectroradiometer (MODIS) land use categories used in our WRF simulation (see details in *Huang et al.* [2013]). The forward simulation using E_{SNEI05} is defined as F_{SNEI05} (Table 2). Two other simulations were conducted in which the CARB ($E_{CARB10v13}$) and NEI 08 (E_{NEI08}) bottom-up anthropogenic emission inventories were used (Table 2):

1. $F_{CARB10v13}$. Same as E_{SNEI05} used in the assimilation, except that the emissions of all sectors in the California grid cells were replaced with the daily varying gridded emission inputs released by CARB in March 2013 (M. Huang et al., personal communication with CARB, 2013). The CARB emissions were projected from the base year of 2008 to 2010, using region- and emissions-category-specific growth and control factors contained in their "California Emissions Projection Analysis Model."
2. F_{NEI08}. NEI 08 (M. Huang et al., personal communication with Harvard University where the NEI 08 inputs for the standard GEOS-Chem simulations were created from the same source emission files developed by U.S. EPA, 2013), which also varies on weekdays and weekends and includes diurnal cycles.

These multiple emission inputs were mass-conservatively regridded into STEM grid using the Model-3 I/O API tools (http://www.cmascenter.org/ioapi/documentation/3.1/html/AA.html#tools), and necessary mapping was conducted for VOC species from the chemical mechanism that each inventory was originally developed upon to SAPRC-99 where necessary. The NO_x emissions in these bottom-up inventories will be compared quantitatively in section 3.2.1.

2.3. The 4D-Var Assimilation Method

We assimilated surface NO_2 and OMI NO_2 columns separately and jointly to update the bottom-up NO_x emissions in each model grid by assimilating surface NO_2 and satellite NO_2 columns (cases A_{SUR}, A_{COL}, and A_{BOTH} in Table 2). The 4D-Var approach is used, which requires the adjoint model of STEM [*Sandu et al.*, 2005], and has been previously applied by *Chai et al.* [2009] to update emission estimates in the Northeastern U.S. by assimilating satellite (i.e., SCIAMACHY) NO_2 columns in a coarser STEM model grid. This method seeks the optimal solution to minimize the cost function J in equation (4) by applying the large-scale bound-constrained

limited-memory Broyden-Fletcher-Goldfarb-Shanno minimization routine [*Zhu et al*., 1997] through a number of iterations, as implemented in STEM by *Chai et al*. [2006, 2007, 2009]. In this study, the optimization proceeds until the cost function is reduced to <0.001 of its initial value or the number of iterations reaches 25.

$$J(\mathbf{x}_0, \varepsilon) = \frac{1}{2}\left(\mathbf{x}_0 - \mathbf{x}_0^{\mathbf{b}}\right)^{\mathrm{T}}\mathbf{B}^{-1}\left(\mathbf{x}_0 - \mathbf{x}_0^{\mathbf{b}}\right) + \frac{1}{2}(\varepsilon - 1)^{\mathrm{T}}\mathbf{E}^{-1}(\varepsilon - 1) + \frac{1}{2}\sum_{i=0}^{N}\left(\mathbf{y_i} - \mathscr{H}(\mathbf{x_i})\right)^{\mathrm{T}}\mathbf{O_i}^{-1}\left(\mathbf{y_i} - \mathscr{H}(\mathbf{x_i})\right) \quad (4)$$

where **B**, **E**, and **O** are error covariance matrices for the model background $\mathbf{x_0}$, for NO_x emission scaling factor ε, and the available observations $\mathbf{y_i}$ (in this study, column or/and surface NO_2) at any instant time t_i within the assimilation window, respectively. The observation operator $\mathscr{H}$ maps the model space **x** onto the observation space. Here we used the similar configurations to those applied by *Chai et al*. [2009] in their basic cases that only controlled NO_x emissions. This means that the second and third terms in equation (4) are considered, which represent a departure from initial emission inventories, and a measure of misfit between the model and observations, respectively. *Chai et al*. [2009] discussed cases that controlled O_3 initial conditions (in which the first term in equation (4) was also counted) together with NO_x emissions and did not find significant improvement in their results. In this study, emission scaling factor was controlled instead of the emission rates for several advantages as described by *Hakami et al*. [2005]. We used a 24 h assimilation window for each day of May 2010, a uniform uncertainty of 0.5 for ε, and the uncorrelated observation errors for surface NO_2 and OMI NO_2 columns. The observation errors for surface NO_2 were based on 20% of the grid-averaged observations that mainly account the uncertainties of the CFs (section 3.1.2). The observation errors for OMI NO_2 were based on the measurement errors included in the KNMI product. Ideally, observation errors should account for both measurement errors and representative errors (e.g., the standard deviation of measurements located in each model grid as defined in *Chai et al*. [2007] or using the superobservation approach as in *Miyazaki et al*. [2012a] and *Eskes et al*. [2003]). In our cases, the representative errors are small in most grid cells and ignored because of the similar spatial scales that the observations and the model resolution represent. Observation errors may not always be uncorrelated, especially for remote sensing L2 data. However, estimating the observation error correlation is still very challenging and has not been widely applied in both weather and chemical assimilation research and operation [*Stewart et al*., 2008, 2013; *Silver et al*., 2013]. For the applications that use dense observations in coarse model grids, sometimes, data thinning (discarding data nearby) and superobbing (grouping data nearby) are performed to compensate the impact of omitting error correlation on assimilation results. As we aim at conducting assimilation on fine model grids, we do not use any of these methods that could cause the loss of information from the observations. The measurement errors are often correlated with the retrieved columns. If the higher retrieved columns are assigned higher errors, then these observations can have smaller influences on the a posteriori. To help reduce the impact of omitting the off-diagonal values in the error covariance matrices, and the possible unrealistic observation errors used in the assimilation, future work will be conducted including the test of constant observation errors, and the assignment of different weights between the multiple terms in J. Complexities introduced from the retrieval processes into satellite L2 retrievals, which affect the assimilation, can ultimately be avoided by the assimilation of satellite L1 products (radiances).

The domain for our assimilation cases is a subdomain (90 × 90 grid boxes, approximate latitude/longitude ranges, ~32–42°N/126–114°W) of the Western U.S. domain. It covers California where the observations were dense during the studied period. The assimilation generated grid-specific daily-varying scaling factors on NO_x emissions in this subdomain. We also conducted simulations over the entire Western U.S. domain with these scaling factors applied to the sub-domain grids (cases F_{SNEI05_ASUR}, F_{SNEI05_ACOL}, and F_{SNEI05_ABOTH} in Table 2), and the resulting chemistry fields over the entire Western U.S. domain were evaluated with independent measurements in the Western U.S. All of the assimilation results are presented on a monthly scale in section 3.2.

2.4. Adjoint Sensitivity Analysis

The distributions of the adjoint variable reflect backward in time the change of chemical distributions of the species or model inputs/parameters that influence a defined response function (e.g., air quality-related metrics such as surface or column NO_2 at any given receptor(s) at a specific time). These values can (1) help understand the specific processes that lead to a state of the atmosphere, (2) identify areas where perturbations/uncertainties in the concentration of the chemical species of interest at earlier times or model

Table 3. Adjoint Sensitivity Analysis Conducted in This Study

Date	Receptor in California[a]	J1 (Column) or J2 (Surface) in Equation ((5))	Temporally Averaged Results Throughout the Day	Instantaneous Results at Selected Times Within the Day
9 May 2010	Long Beach	J2	Y	N
9 May 2010	Long Beach	J1	Y	N
9 May 2010	Riverside	J1	Y	Y, at 01, 08 and 15 UTC
9 May 2010	Joshua Tree National Park	J1	Y	N
16 May 2010	Long Beach	J2	Y	N
16 May 2010	Long Beach	J1	Y	N

[a]The respective center latitude/longitude/elevation of the model grid boxes at Long Beach, Riverside, and Joshua Tree National Park are 33.7°N/118.2°W/7.5 m, 33.9°N/117.5°W/336.7 m, and 33.8°N/115.9°W/871.8 m.

inputs/parameters will result in significant changes in the defined response function, and (3) help interpret the 4D-Var assimilation results. Adjoint sensitivity analyses have been applied in a number of previous studies from global to regional scales for gases and aerosols [e.g., *Chai et al*., 2006; *Zhang et al*., 2009; *Kopacz et al*., 2011; *Zoogman et al*., 2011; *Carmichael et al*., 2008; *Hakami et al*., 2006; *Bowman and Henze*, 2012; *Huang et al*., 2013; *Lapina et al*., 2014].

In this study, we use adjoint sensitivity to demonstrate what NO_x emission sources influence the modeled surface or column NO_2 (defined as the response function J_i in equation (5)) in the selected grid box(es) close to the OMI overpass time (22 UTC) on 9 May and 16 May to represent the windy and stagnant weather conditions, respectively (Table 3).

$$\lambda_{E_{NO_x}} = \frac{\partial J_i}{\partial E_{NO_x}} \frac{E_{NO_x}}{J_i} \tag{5}$$

where i = 1 or 2 denotes the response function for column or surface NO_2, respectively. The normalized adjoint sensitivity $\lambda_{E_{NO_x}}$ in equation (5) is a function of time and space, and we will present results temporally averaged through the studied days and those at selected times within the studied period (Table 3).

The Long Beach area has one of the world's largest ports, and its air quality is affected by both maritime (mainly shipping) and terrestrial emissions in SoCal [*Huang et al*., 2011]. Similar to the findings by *Brioude et al*. [2013], our assimilation results indicate significant emission changes in 2005–2010 around the Long Beach area (details in section 3.2). Therefore, we will be focusing on results from the Long Beach case study. To discuss the impact of receptor locations on the spatial distributions of $\lambda_{E_{NO_x}}$, on the windy day of 9 May, two additional cases were conducted in which Riverside and Joshua Tree National Park are selected to be the receptor grid boxes, respectively (Table 3). Both locations suffer from chronic air pollution, in part affected by emission sources in upwind inland areas such as the Greater LA.

3. Results and Discussion

3.1. Evaluation of the Modeled NO_2 and CFs in the F_{SNEI05} Case

3.1.1. Evaluation of NO_2 Spatial Distributions

Figures 2a–2c compare the modeled NO_2 from the F_{SNEI05} case with OMI tropospheric NO_2 columns, surface NO_2 (after the model-based CFs were applied to the original measurements), and the near-surface aircraft NO_2 measurements, respectively. Although the maximum numbers of observations in each grid for surface (>1000), aircraft (>50), and column NO_2 (~5) vary significantly in this month, the three sets of comparisons show qualitatively similar spatial distributions of the model biases: The model overpredicts NO_2 over the populated regions such as South Coast, Fresno, and the Bay Area by up to >50%, indicating the errors in the a priori emission inventory and the model chemistry. NO_2 is generally underpredicted by up to a factor of >5 over the remote regions where NO_2 concentrations are low, as a result of the underpredicted transported background NO_2 and the uncertainties in the model chemistry. The correlation coefficient *r*, root-mean-square-error (RMSE) and mean absolute error (MAE) for each pair of comparison were derived from the model grid-averaged data (Table 4). The spatial distributions of modeled and observed NO_2 are indicated to have best and worst consistency with surface ($r = 0.84$; RMSE/MAE = 49%/38% of the observed mean values) and aircraft ($r = 0.53$; RMSE/MAE = 130%/72% of the observed mean values) observations, respectively. This is

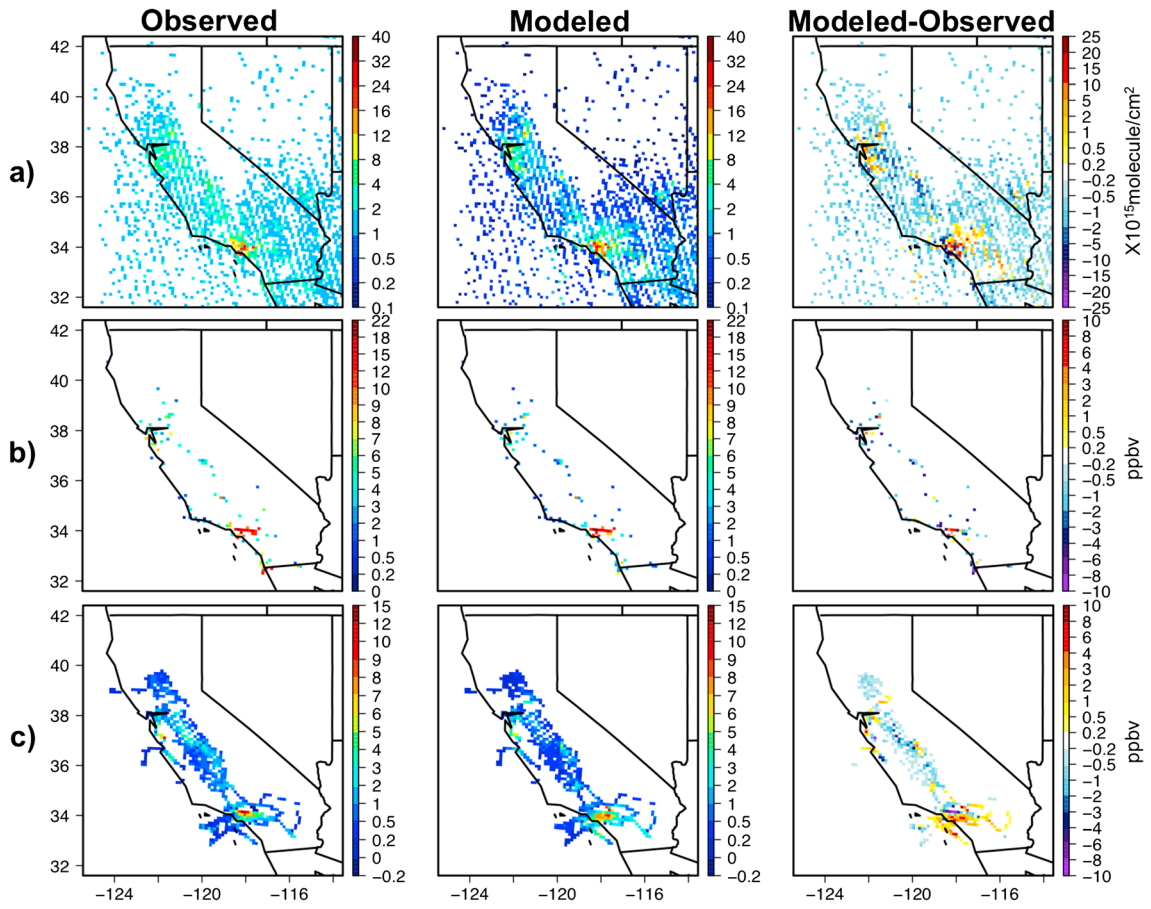

Figure 2. Evaluation of the modeled NO_2 a priori fields in May 2010. The modeled NO_2 fields were compared with (a) OMI tropospheric NO_2 columns, (b) bias-corrected surface NO_2, and (c) aircraft near-surface (<2 km agl) NO_2 measurements. Statistics for the evaluation are in Table 4.

possibly due to the different sampling densities. In all comparisons, MAE values are 31%–44% lower than the RMSEs, indicating moderate variances in the individual errors. In the comparisons with observed surface and column NO_2 which are associated with relatively larger observation errors, ~15% and ~34% of the model errors fall within the observation errors, respectively.

3.1.2. Evaluation of the CFs

To evaluate the CFs used to correct the surface NO_2 observations (mentioned in section 2.1.2) and to estimate the observation errors of the bias-corrected surface NO_2 used in the assimilation case A_{SUR}, we compare the observed and model-based CF values, calculated using equation (3) along the near-surface flight tracks (Figures 3a and 3b). Note that the observation-based CFs represent the higher bound of the CFs, as the observed ANs do not include the multifunctional or long-chain ANs and therefore are not identical to the actual total ANs and the lumped organic nitrates treated in the model. The CFs are >0.8 in a few urban

Table 4. Evaluation of the Modeled NO_2 Fields in Case F_{SNEI05} With OMI, Surface, and Aircraft Measurements[a]

Observations Compared	*r*	Mean Observation	RMSE	MAE
OMI NO_2 columns (within the assimilation domain)	0.63	2.04	1.97 (97%)	1.28 (63%)
OMI NO_2 columns (California only)	0.62	2.38	2.36 (99%)	1.44 (60%)
Bias-corrected surface NO_2	0.84	5.98	2.94 (49%)	2.25 (38%)
Aircraft near-surface NO_2	0.53	1.15	1.49 (130%)	0.83 (72%)

[a]The units of mean observations, RMSEs, and MAEs are the same as the compared observations (i.e., $\times 10^{15}$ molecule/cm^2 for OMI columns; ppbv for surface and aircraft measurements), and *r* is unitless. Values in the parentheses indicate the % of the mean observed values.

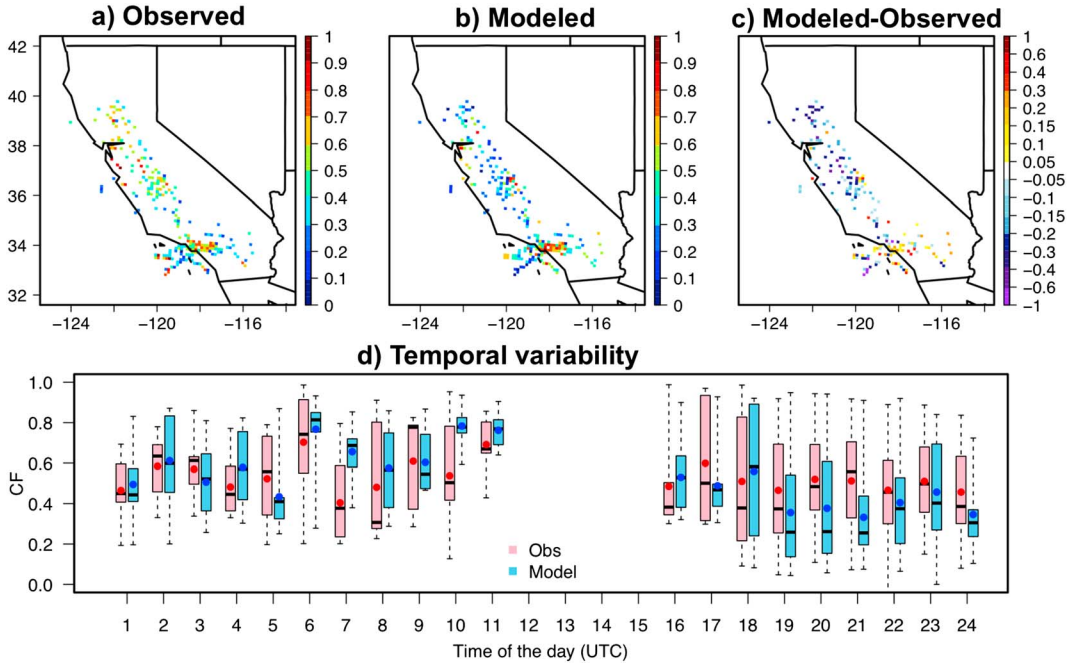

Figure 3. Evaluation of the modeled bias correcting factors (CFs) with those calculated based on the aircraft near-surface (<2 km agl) observations: (a) observed and (b) modeled CFs along the flight tracks and (c) their differences. These data were temporally averaged in each model grid box. (d) The temporal variability of observed (pink) and modeled (light blue) CF values, shown as box-and-whisker plots (minimum, first quartile, medium, third quartile, maximum). The data are binned with an hourly interval, and the mean values for data in each bin are shown as red and blue dots for observed and modeled CFs, respectively.

regions (South Coast, Fresno, Sacramento, and the Bay Area), while they can be as low as <0.3 in many rural and remote areas where plumes are typically aged and NO_z ($NO_z = NO_y - NO_x$) species make larger contributions to NO_y. The model-based CFs show similar spatial variability to the observations, with correlation coefficient *r* and RMSE of 0.55 and 0.24, respectively, >70% of which differing from the observations by no larger than ±0.20. The CFs are generally overpredicted over the urban regions and underpredicted in the Central Valley (Figure 3c). Over SoCal, the CFs are close to the previous calculations by a regional model(Comprehensive Air Quality Model with Extensions) for the year 2005 [*Bechle et al*., 2013] and higher than the GEOS-Chem results at the OMI overpass times in Spring 2005 [*Lamsal et al*., 2008] due to the different time periods studied and model resolutions used. To evaluate the model's capability of capturing the observed temporal variability, the data on all flight days in May 2010 were binned with an hourly interval. The observed and modeled CFs are shown as box-and-whisker plots for each time bin, indicating fairly good consistency (discrepancies of the hourly mean values <0.20) in most time bins (Figure 3d). Based on the evaluation of modeled CF fields, we estimate the observation errors used in the assimilation case A_{SUR} to be ~20%. The uncertainties shown in the modeled CFs were influenced by a number of reasons such as the a priori NO_y emissions, transport, and the model chemistry, which can also be the sources of uncertainty in the 4D-Var results.

3.2. Inversion Results

3.2.1. Updated Emission Estimates and the Implications of Emission Trends

The separate (cases A_{COL} and A_{SUR}) and joint (case A_{BOTH}) assimilation of column and surface NO_2 generated three sets of grid-specific NO_x emission scaling factors for each day of May 2010. We first analyze results in cases A_{SUR} and A_{COL}. The monthly mean relative changes in NO_x emissions (RC_{NOx}) from the a priori are shown in Figures 4a and 4b for cases A_{COL} and A_{SUR}, respectively. In both cases, the updates in NO_x emissions mainly occur in the Greater LA region, the Bay Area, and the Central Valley where the emissions are high and dominantly from the mobile sources. These results indicate that the applied emission control strategies to this emission sector during the past years effectively changed the NO_x emissions in these regions. The RC_{NOx}

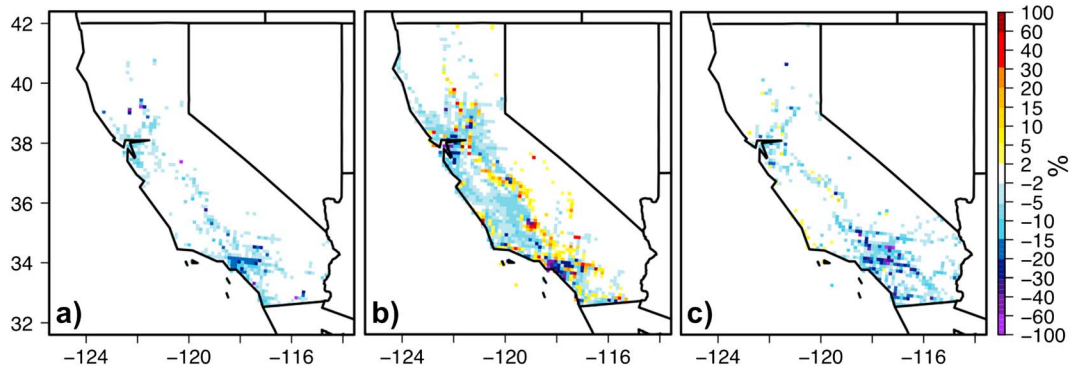

Figure 4. The relative changes (%) from the a priori NO_x emission estimates made in (a) case A_{COL} that assimilated OMI NO_2 columns and (b) case A_{SUR} that assimilated surface NO_2. (c) The differences in a posteriori NO_x emissions between the A_{BOTH} and A_{SUR} cases, scaled by a factor of 5 (i.e., $5 \times (E_{ABOTH} - E_{ASUR})$). Cases were defined in Table 2.

generated in the A_{SUR} case overall show stronger spatial variability than in the A_{COL} case. This is mainly due to the significantly (i.e., tens to hundreds of times) larger number of surface observations assimilated, which is primarily affected by the different sampling time frequency. Other factors also contribute to the different results in the A_{COL} and A_{SUR} cases. For example, the method to correct the biases in surface NO_2 may have led to the opposite signs of RC_{NOx} values in the Central Valley and some suburban areas in SoCal. Omitting bias correction on OMI NO_2 observations can introduce biases to the results in case A_{COL}. In addition, modeled column and surface NO_2 at a given receptor grid can be sensitive to NO_x emission sources at different locations, as shown in the adjoint sensitivity analysis to be presented in section 3.2.3. The RC_{NOx} values that resulted from jointly assimilating surface and column NO_2 (case A_{BOTH}) are closer to those in case A_{SUR} than case A_{COL}, indicating the stronger control in the joint assimilation by the larger number of surface observations. Overall, the RC_{NOx} values in case A_{BOTH} indicate larger reductions from the a priori than results in cases A_{COL} and A_{SUR} (Figure 4c; note that the differences were scaled by 5 in the figure), most notably in SoCal and the Bay Area.

The spatial distributions of NO_x emissions in various bottom-up and top-down inventories ($E_{CARB10v13}$, E_{NEI08}, and the a posteriori estimates) are compared against E_{NEI05} and illustrated in Figure 5. These inventories all indicate decreases in NO_x emissions from E_{NEI05} over multiple urban areas (e.g., the Greater LA and Bay Area, Sacramento, Fresno, and Bakersfield). Over many rural and remote regions, the a posteriori estimates do not show higher NO_x emissions than E_{NEI05} as $E_{CARB10v13}$ and E_{NEI08} demonstrate, and E_{NEI08} shows the highest positive differences from E_{NEI05}. The differences of NO_x emissions in these inventories were quantified over large spatial scales and summarized in Table 5a. Over the entire state, the A_{COL}, A_{SUR}, and A_{BOTH} cases lowered the a priori by ~8%, ~11%, and ~13%, respectively. These indicate reductions in E_{NEI05} by ~26%, ~29%, and ~30%, respectively. The agreement in the three sets of a posteriori estimates statewide (<4% of differences) results from the offsetting in their different spatial distributions as shown in Figure 5. These a posteriori estimates are significantly lower than those in E_{NEI08} (~4% reduction from E_{NEI05}) as they represent different base years. These large differences indicate that the strongest decreases in emissions during 2005–2010 occurred after the economic recession started since late 2007. The a posteriori estimates are similar to those in $E_{CARB10v13}$, which indicates a statewide ~30% reduction from E_{NEI05}. This consistency strengthens our confidence in the used 4D-Var assimilation system, as well as in CARB's emission projection system, for the purposes of studying emission trends on relative large spatial scales.

Our E_{ACOL} indicates ~7% larger NO_x emission reduction during 2005–2010 than E_{Lamsal} (i.e., those derived from the emission scaling factor product created by Lamsal et al. in Figure S1, using GEOS-Chem on a $1° \times 1.25°$ horizontal resolution grid) for four major reasons: (1) the used model and its resolution: As suggested in previous studies over the North America, regional models on a 4–12 km horizontal resolution can better capture pollutants' spatial gradients and interpret satellite data [e.g., *Valin et al*., 2011; *Fishman et al*., 2011], and our results indicate that such factors can also affect the accuracy in top-down emission estimates, (2) the used top-down methodology: The 4D-Var method in this study takes account of important

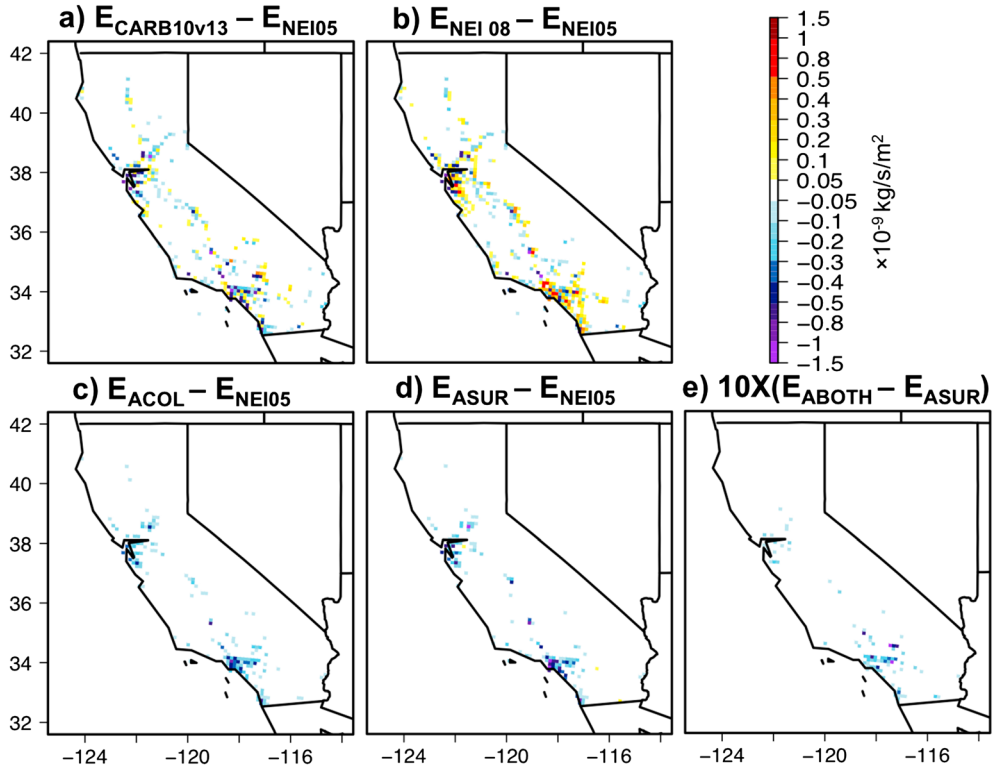

Figure 5. Differences between NO_x emissions in multiple inventories and the NEI 05: (a) $E_{CARB10v13} - E_{NEI05}$, (b) $E_{NEI08} - E_{NEI05}$, (c) $E_{ACOL} - E_{NEI05}$, (d) $E_{ASUR} - E_{NEI05}$, and (e) $10 \times (E_{ABOTH} - E_{ASUR})$. Emission inventories were defined in Table 2.

atmospheric processes which are ignored in the mass balance types of approaches, such as transport and chemical transformation, (3) the studied period: E_{Lamsal} and our a posteriori estimates are annual mean and monthly mean based, respectively, and (4) the used OMI data version and filtering criteria: E_{Lamsal} may be generated using an earlier version of OMI data than the KNMI v2.0 used in this study, which can be associated with different uncertainties. E_{Lamsal} only focused over areas dominantly affected by anthropogenic emission sources (i.e., contributing to >50% of the total emissions). Our study also considers areas dominantly affected by nonanthropogenic emission sources. As emissions in these regions contribute little to the statewide total emissions, this factor is not a major contributor. Future work is suggested to prioritize the impact of each factor on the differences between E_{ACOL} and E_{Lamsal}.

Lamsal et al. [2011] calculated a "beta" term, defined as the ratio of the changes in surface NO_x emissions and the changes in modeled tropospheric NO_2 columns in 2006, based on their GEOS-Chem base simulation and a sensitivity simulation in which the anthropogenic NO_x emissions were perturbed by 15%. In California, their beta values range from ~0.7 to ~1.2. In this study, the ratio of the changes in the monthly mean

Table 5a. Differences (in Percent) in Statewide and Subregional[a] NO_x Emissions Between Multiple Sets of Emission Estimates and E_{NEI05}[b]

Emission Estimates	Statewide	SoCal	CenCal	NoCal
$E_{CARB10v13}$	−30.46	−34.80	−24.85	−28.66
E_{NEI08}	−3.75	4.57	−9.00	−15.79
E_{Lamsal}	−19.53	−21.69	−21.77	−5.13
E_{ACOL}	−26.42	−29.63	−24.00	−22.39
E_{ASUR}	−28.58	−30.82	−27.88	−24.25
E_{ABOTH}	−30.02	−33.22	−28.38	−24.78

[a]Definitions of the subregions: SoCal (southern California), south of 35°N; CenCal (central California), 35–38°N; NoCal (northern California), north of 38°N. These subregions contribute to ~49%, ~31%, and ~20% of the statewide a priori NO_x emissions, respectively.
[b]The full descriptions for each emission data set are in Table 2.

Table 5b. Differences (in Percent) in Urban and Nonurban NO_x Emissions Between Multiple Sets of Emission Estimates and E_{NEI05}[a]

Emission Estimates	Urban	Nonurban
$E_{CARB10v13}$	−40.57	−20.16
E_{NEI08}	−11.71	4.36
E_{ACOL}	−30.29	−22.47
E_{ASUR}	−37.42	−19.58
E_{ABOTH}	−39.06	−20.81

[a]The definitions of urban and nonurban regions in California are consistent with those in the WRF model simulation, as shown in Figure 1c.

California NO_x emissions in case A_{COL}, over the changes in the modeled column NO_2, turns out to be ~0.9. The differences and uncertainties of this relationship in both studies, resulting from the different top-down approaches, models, and studied periods, are worth further investigation.

The differences of NO_x emissions in these inventories were then quantified over three subregions (i.e., SoCal, CenCal, and NoCal) in Table 5a. Over the SoCal region (south of ~35°N) that contributes to almost half of the total NO_x emissions in California in the a priori emissions, the A_{COL}, A_{SUR}, and A_{BOTH} cases lowered the a priori by ~12%, ~14%, and ~17%, respectively, corresponding to the reductions from E_{NEI05} by ~30%, ~31%, and ~33%. These reductions are larger than those over the entire state, but similarly, they are most significantly different from E_{NEI08}, which indicates a ~5% of increase. They are also close to (<5% smaller than) the ~35% of emission reduction indicated by $E_{CARB10v13}$ and again moderately differ from E_{Lamsal}, which lowered E_{NEI05} by ~22%. The reduction in NO_y emissions indicated by *Brioude et al.* [2013] (~27% for a smaller region in SoCal) and our a posteriori estimates over SoCal are similar, suggesting that chemical transformation (not considered in the former study) and the types of observations integrated (aircraft data in the former study; surface or/and satellite data in our cases) may not always be the controlling factors when deriving the top-down NO_x emission estimates over large spatial and temporal scales. These conclusions are based on our monthly results over SoCal where fresh plumes were dominant and dense observations were available and need to be further validated for other regions/periods.

Over the CenCal (35–38°N) and NoCal (north of ~38°N) regions that contribute to 31% and 20% of the statewide total NO_x emissions in the a priori, compared to independent inventories, all three a posteriori estimates are also closer to $E_{CARB10v13}$ than E_{Lamsal} and E_{NEI08}. Among the three a posteriori estimates, again E_{ACOL} and E_{ABOTH} indicate the lowest and highest reductions from E_{NEI05}, respectively. E_{ACOL} is the closest to $E_{CARB10v13}$ over CenCal, in contrast to its largest differences from $E_{CARB10v13}$ over SoCal, NoCal, and the entire state.

The differences of NO_x emissions in these inventories were also summarized for California's urban (as defined in Figure 1c) and nonurban regions in Table 5b. In the urban regions, the three a posteriori estimates all indicate more than 30% of decreases from E_{NEI05}, significantly greater than the ~12% of reduction indicated by E_{NEI08}. E_{ACOL} and E_{ABOTH} indicate the lowest (~30%) and highest (~39%) reductions from E_{NEI05}, respectively, and E_{ABOTH} shows the smallest discrepancy from $E_{CARB10v13}$ (~40%). Over the much broader nonurban areas, the changes in emissions from E_{NEI05} are, in general, less strong. $E_{CARB10v13}$, E_{ACOL}, E_{SUR}, and E_{ABOTH} indicate similar reductions (20–22%), in contrast to the increase of ~4% indicated by E_{NEI08}. Among the three a posteriori estimates, again, E_{ABOTH} shows the smallest discrepancy from $E_{CARB10v13}$, and E_{ACOL} suggests ~3% larger reductions than E_{ASUR}.

3.2.2. Cross Validation of NO_2 and O_3 Fields With Aircraft Measurements

The STEM-modeled NO_2 and O_3 fields in the simulations using various sets of emission estimates are compared against the observed NO_2 and O_3 along WP-3D flight tracks near the surface in this month. The spatial patterns of model errors ($|C_{model}-C_{obs}|$) in case F_{SNEI05} and the rest of the simulations are shown in Figures S3 and S4 for NO_2 and O_3, respectively. The modeled NO_y were also compared with the aircraft measurements, and the spatial patterns of the differences in modeled NO_y errors are qualitatively similar to those of NO_2 over many regions (not shown). Three statistical metrics (*r*, RMSE, and MAE) to evaluate these simulations are summarized in Table 6 over the entire state and three subregions.

We first evaluate the effectiveness of assimilation by comparing case F_{SNEI05} with the F_{SNEI05_ASUR}, F_{SNEI05_ACOL}, and F_{SNEI05_ABOTH} cases. Errors in modeled NO_2 a posteriori dropped over most urban regions while increased over many rural areas in the Central Valley, and F_{SNEI05_ASUR} shows the largest increases in modeled NO_2 errors over these rural regions among the three a posteriori (Figure S3). On large spatial scales, referring to case F_{SNEI05}, the use of the a posteriori emission estimates lowered the modeled NO_2 discrepancies along the flight tracks over the entire state (Table 6). In contrast to SoCal and NoCal, the a

Table 6. Statistics of the Model Evaluation Against Aircraft Near-Surface NO_2 and O_3 Measurements in California for Various Forward Simulations (Definitions in Table 2)[a]

		NO_2			O_3		
Regions	Cases	*r*	RMSE (ppbv)	MAE (ppbv)	*r*	RMSE (ppbv)	MAE (ppbv)
Statewide	F_{SNEI05}	0.53	1.49	0.83	0.58	11.44	8.67
	$F_{CARB10v13}$	0.51	1.42	**0.76**	**0.60**	**9.89**	**7.91**
	F_{NEI08}	0.50	1.76	0.95	0.51	16.13	11.50
	F_{SNEI05_ACOL}	**0.57** (+)	**1.34** (+)	0.78 (+)	0.52 (−)	11.72 (−)	9.11 (−)
	F_{SNEI05_ASUR}	0.48 (−)	1.44 (+)	0.78 (+)	0.58 (+)	11.16 (+)	8.53 (+)
	F_{SNEI05_ABOTH}	0.48 (−)	1.44 (+)	0.78 (+)	0.58 (+)	11.15 (+)	8.54 (+)
SoCal	F_{SNEI05}	0.49	2.37	1.45	**0.52**	13.59	9.71
	$F_{CARB10v13}$	0.48	2.24	1.34	0.47	**9.33**	**7.18**
	F_{NEI08}	0.49	2.85	1.76	0.46	22.47	16.62
	F_{SNEI05_ACOL}	**0.58** (+)	**1.96** (+)	**1.20** (+)	0.48 (−)	12.31 (+)	8.89 (+)
	F_{SNEI05_ASUR}	0.36 (−)	2.35 (+)	1.38 (+)	0.48 (−)	12.81 (+)	9.29 (+)
	F_{SNEI05_ABOTH}	0.36 (−)	2.35 (+)	1.38 (+)	0.48 (−)	12.73 (+)	9.23 (+)
CenCal	F_{SNEI05}	0.50	1.15	0.69	0.15	12.21	9.70
	$F_{CARB10v13}$	0.50	**1.11**	**0.63**	**0.27**	**11.27**	**9.39**
	F_{NEI08}	0.46	1.24	0.75	0.06	15.74	11.38
	F_{SNEI05_ACOL}	**0.55** (+)	1.14 (+)	0.71 (−)	−0.07 (−)	13.59 (−)	11.30 (−)
	F_{SNEI05_ASUR}	0.45 (−)	1.20 (−)	0.73 (−)	0.22 (+)	12.12 (+)	9.66 (+)
	F_{SNEI05_ABOTH}	0.45 (−)	1.20 (−)	0.73 (−)	0.22 (+)	12.12 (+)	9.67 (+)
NoCal	F_{SNEI05}	0.46	0.60	0.40	**0.53**	8.32	6.65
	$F_{CARB10v13}$	0.55	**0.45**	**0.34**	0.46	**7.56**	**6.09**
	F_{NEI08}	0.49	0.54	0.39	0.51	10.31	8.04
	F_{SNEI05_ACOL}	0.51 (+)	0.53 (+)	0.38 (+)	0.53 (−)	8.26 (+)	6.60 (+)
	F_{SNEI05_ASUR}	0.54 (+)	0.48 (+)	0.36 (+)	0.53 (−)	8.14 (+)	6.47 (+)
	F_{SNEI05_ABOTH}	**0.57** (+)	0.46 (+)	0.34 (+)	0.53 (−)	8.21 (+)	6.55 (+)

[a]The best cases (with higher *r* values/lower errors) are in bold, and whether the assimilation improved (+) or exacerbated (−) the model performance (relative to case F_{SNEI05}) is indicated. The subregions were defined in Table 5a.

posteriori emissions led to higher modeled NO_2 errors along the flight tracks in CenCal, especially in the F_{SNEI05_ASUR} and F_{SNEI05_ABOTH} cases. This can be due to the more uncertain and sparse monitoring data that we assimilated, as well as the complex meteorology, topography, and plume ages that the model may not represent well in this region. The changes in modeled O_3 and its uncertainties can be affected by those in NO_x (and other precursors') emissions, as well as other factors such as the chemical regimes of the studied regions. Over the NO_x-limited areas, the lower a posteriori NO_x emissions led to decreases in modeled O_3 fields, resulting in reduced modeled O_3 errors near Fresno, Bakersfield, and rural areas in SoCal, where O_3 concentrations were overpredicted in the F_{SNEI05} case and increased modeled O_3 errors over some rural areas in the Central Valley where O_3 concentrations were underpredicted in the F_{SNEI05} case. The lower a posteriori NO_x emissions caused larger errors in NO_x-saturated regions such as the Greater LA areas, where O_3 concentrations were overpredicted in the F_{SNEI05} case (Figure S4). The modeled O_3 errors were reduced on large spatial scales, except in the F_{SNEI05_ACOL} case over the CenCal region (Table 6). Discussions on modeled O_3 will be continued in section 3.2.4, focusing on the surface.

The modeled NO_2 and O_3 fields using independent bottom-up inventories ($F_{CARB10v13}$ and F_{NEI08}) were also evaluated with the aircraft observations and compared with the evaluation of our a posteriori chemical fields. The differences in modeled NO_2 and O_3 errors between F_{NEI08} and F_{SNEI05} vastly disagree with those in the other pairs of comparison (Figures S3 and S4). On large spatial scales, case F_{NEI08} results in the largest discrepancies from the aircraft observations among all simulations, and case $F_{CARB10v13}$ generates closer NO_2 and O_3 fields to the aircraft measurements than those in case F_{SNEI05}. The spatial patterns of differences in model errors between $F_{CARB10v13}$, F_{SNEI05_ASUR}, F_{SNEI05_ACOL}, F_{SNEI05_ABOTH}, and F_{SNEI05} are qualitatively similar over certain regions such as SoCal and Fresno (Figures S3 and S4), but overall, no strong correlations were found. This indicates that the updates on NO_x emissions by integrating monitoring data qualitatively match those by using CARB's bottom-up emission projection model to some extent, which was indeed reflected in Figure 5. However, the a posteriori estimates still notably differ from $E_{CARB10v13}$ on small spatial

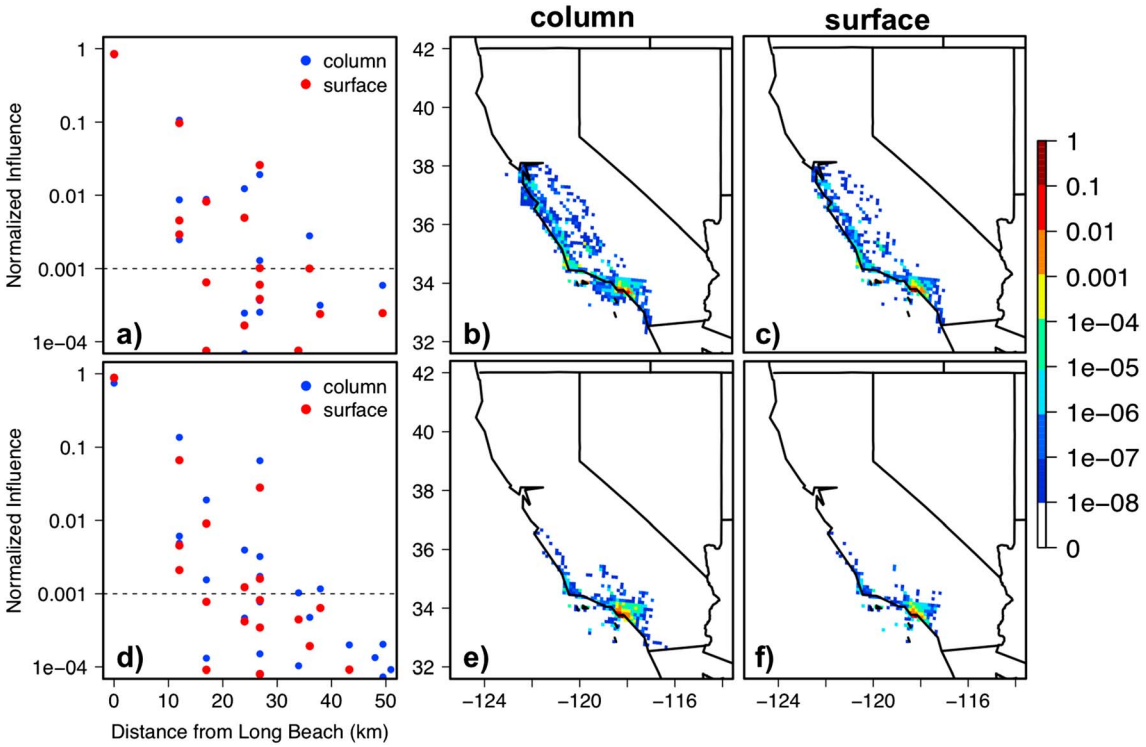

Figure 6. Adjoint sensitivity (fractions of total are shown) of Long Beach (b, e) column and (c, f) surface NO_2 at 22 UTC (near OMI overpass time) on 9 May (Figures 6b and 6c) and 16 May (Figures 6e and 6f) 2010 to the same day (temporally averaged during 0–22 UTC) surface NO_x emissions in the model domain. (a, d) The fractions of temporally averaged sensitivity in each grid were shown as a function of distance from the Long Beach model grid. The differences in adjoint sensitivities on 2 days are due to the meteorological conditions.

scales. Overall, case F_{SNEI05_ACOL} shows the best performance in modeled NO_2 over the entire state and SoCal but not as good as case $F_{CARB10v13}$ in NoCal and CenCal. This can be due to the smaller number/worse coverage of the observations we assimilated and the challenges of well-simulating complex atmospheric processes over these areas. The $F_{CARB10v13}$ case also, in general, shows the best performance in modeled O_3, in that the emissions of non-NO_x O_3 precursors (such as VOCs and CO) in $E_{CARB10v13}$ are most up-to-date. Further efforts should be devoted to interpreting the similarities and differences in $E_{CARB10v13}$ and the a posteriori estimates and integrating observations to update the emissions of non-NO_x species.

3.2.3. Emissions Affecting the Column and Surface NO_2: Case Studies

The impacts of same-day NO_x emissions on modeled NO_2 are interpreted by the adjoint sensitivity $\lambda_{E_{NO_x}}$. In separate adjoint cases, we define the column and surface NO_2 at 22 UTC in the Long Beach grid as the response functions J1 and J2 in equation (5), and the spatial distributions of $\lambda_{E_{NO_x}}$ can help explain the different 4D-Var results in cases A_{SUR} and A_{COL}. Improvement in air quality in Long Beach area can benefit from emission control from ocean-going vessels, various emission sources around the port (http://www.polb.com/environment/air/emissions.asp), and sources (primarily mobile) from other regions inland. Therefore, we chose this location to be the receptor in the adjoint case study, and the adjoint results on 9 May (Figures 6a–6c) and 16 May (Figures 6d–6f) are contrasted to discuss the effects of meteorological conditions. The surface $\lambda_{E_{NO_x}}$ values in each horizontal grid were averaged from 00 to 22 UTC of the same day, and their spatial distributions are illustrated for the column (Figures 6b and 6e) and surface adjoint cases (Figures 6c and 6f). The temporally averaged $\lambda_{E_{NO_x}}$ values in each grid were plotted as a function of their distances from the Long Beach grid (Figures 6a and 6d).

The modeled surface and column NO_2 in Long Beach grid on both days are shown to be most sensitive to the same-day NO_x emissions within ~40 km (where the temporally averaged normalized $\lambda_{E_{NO_x}}$ values are >0.001), including sources from both maritime and terrestrial regions. Due to the stronger impact of regional

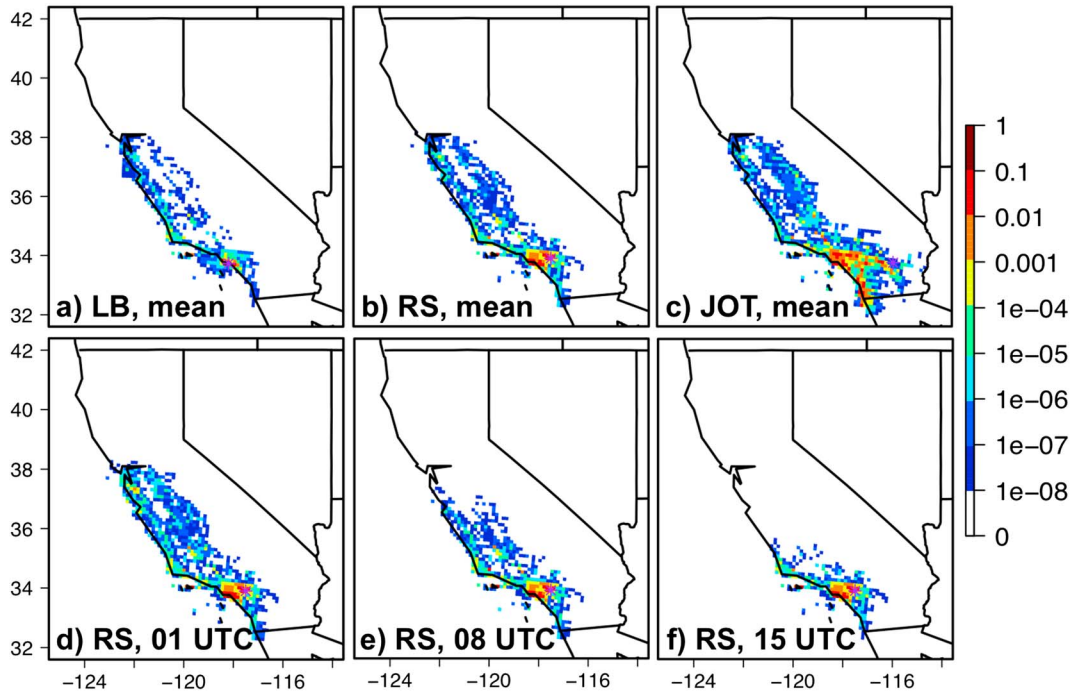

Figure 7. Adjoint sensitivity (fractions of total are shown) of column NO_2 at 22 UTC on 9 May 2010 at (a) Long Beach (LB), (b) Riverside (RS), and (c) Joshua Tree National Park (JOT) to the same day (temporally averaged during 0–22 UTC) surface NO_x emissions in the model domain. Adjoint sensitivity of column NO_2 at 22 UTC on 9 May 2010 at RS to surface NO_x emissions in the model domain at (d) 01 UTC, (e) 08 UTC, and (f) 15 UTC. Purple stars in each figure indicate the receptor grid box.

transport, the column NO_2 in Long Beach is sensitive to NO_x emissions over slightly broader regions than its surface NO_2. The differences in the $\lambda_{E_{NO_x}}$ spatial distributions on these 2 days and between the column and surface cases vary and depend on the meteorological conditions that control the regional transport patterns and chemical transformation. On the windy day of 9 May, surface and column NO_2 in Long Beach were affected by farther emission sources than on a more stagnant day of 16 May. The differences in $\lambda_{E_{NO_x}}$ between the column and surface cases are larger over the South Coast region on 16 May due to the impacts of regional aged plumes.

Brioude et al. [2013] found that NO_y emissions near the port regions in SoCal dropped by a factor of ~5 in 2005–2010 by integrating aircraft measurements on multiple days during CalNex. Our assimilation reduced the E_{SNEI05} in the grids around the Long Beach area (averaged in a 3×3 kernel with the Long Beach grid box in the center) by 33%, 56%, and 57% in the A_{COL}, A_{SUR}, and A_{BOTH} cases, respectively. These differences over the Long Beach area indicate that the types of assimilated observations can significantly affect the a posteriori emission estimates on small spatial scales. The adjoint sensitivity cases here only partially explain the different monthly RC_{NOx} in various assimilation cases. As discussed in section 3.2.1, other factors such as different observational sampling strategies and their uncertainties also contribute. Untangling the impacts from individual factors in future will benefit the improvement in observing systems and the assimilation results.

We also explore the impact of receptor locations on the spatial distributions of $\lambda_{E_{NO_x}}$. In two additional adjoint cases, we define the response functions to be column NO_2 at 22 UTC on the windy day 9 May in Riverside (RS) and Joshua Tree National Park (JOT) grid boxes, respectively. The spatial distributions of the temporally averaged $\lambda_{E_{NO_x}}$ in these cases are shown in Figures 7b and 7c to compare with those in the Long Beach case (Figure 7a, same as Figure 6b). Due to the stronger impact of regional pollution transport, the modeled column NO_2 in both receptor grid boxes on this day are shown to be strongly (normalized $\lambda_{E_{NO_x}}$ values >0.001) sensitive to the same-day NO_x emissions in the Greater LA regions. Column NO_2 in the JOT grid box is also highly sensitive to the same-day NO_x emissions in other California urban regions such as San Diego,

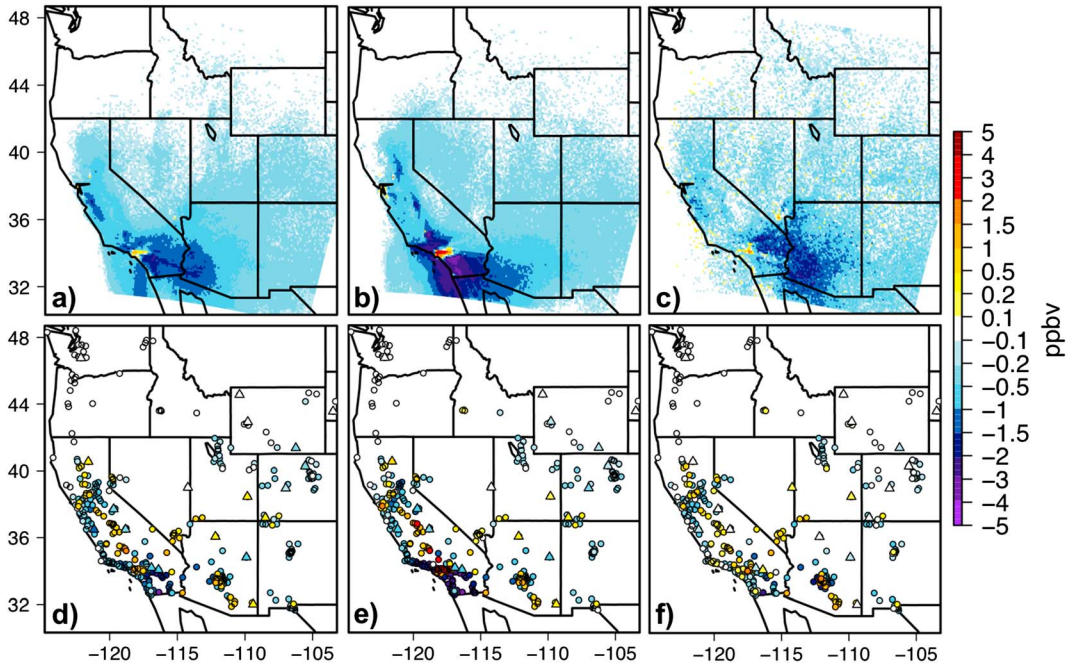

Figure 8. Impact of assimilating (a, d) column NO_2 (case F_{SNEI05_ACOL}) and (b, e) surface NO_2 (case F_{SNEI05_ASUR}) on modeled monthly mean daily maximum 8 h average (MDA8) O_3 over the Western U.S., relative to case F_{SNEI05}. (c, f) Compare MDA8 O_3 in cases F_{SNEI05_ABOTH} and F_{SNEI05_ASUR}, scaled by 5. Figures 8a–8c show the absolute differences, averaged throughout the month; Figures 8d–8f show the changes in model errors ($|C_{model} - C_{obs}|$) at the AQS (circles) and CASTNET (triangles) surface sites, averaged only for the days that observations were available at each site.

Bakersfield, and Fresno that are hundreds of kilometers away. Figures 7d–7f show that nearby sources affect modeled column NO_2 in the RS grid box a few hours after being emitted, and it takes longer than half a day for the farther emission sources (e.g., those in the Bay Area) to be transported to SoCal receptor sites and affect the modeled column NO_2 there. This example demonstrates that the length of simulation window can affect the adjoint sensitivity calculations as well as the 4D-Var results.

Our analysis indicates that over areas similar to Long Beach that are mainly affected by weak winds and fresh plumes, the mass balance types of approaches [e.g., *Martin et al*., 2003] in grid horizontal resolutions coarser than ~40 km may be reasonable for updating NO_x emissions using the observations of the similar spatial resolutions. As the footprints (i.e., the ground scenes detected by satellites) of future geostationary satellites over the North America are designed to be much smaller (e.g., ~4 km for TEMPO and GEO-CAPE) [*Chance et al*., 2013; *Fishman et al*., 2012] and the model resolutions tend to become finer (as also suggested in section 3.2.1), advanced top-down approach such as the 4D-Var assimilation method should be applied to improve the emission estimates, which accounts for the complex chemical transport and transformation processes. The 4D-Var method can also overcome the limitations in the mass balance approaches to study the regions affected by a mixture of local emissions and regional transported plumes such as RS and JOT. The strong sensitivities within the widespread distances of ~40 km to hundreds of kilometers are still smaller than those generated in a global model analysis by *Turner et al.* [2012]. As Figure 7 indicates, this difference can be due to the different simulation windows (~1 day versus 3 weeks) and the defined receptor regions (several model grid boxes versus multiple continents), but it can also be affected by model resolution and domain (12 km in the Western U.S. versus 2° × 2.5° globally).

3.2.4. Impacts of Emission Updates on Modeled Monthly Mean Daily Maximum 8 h Average O_3

The impacts of updated California NO_x emissions on surface O_3 in the Western U.S. are also evaluated. The differences ($F_{SNEI05\_ACOL} - F_{SNEI05}$ and $F_{SNEI05\_ASUR} - F_{SNEI05}$) in monthly mean daily maximum 8 h average (MDA8, NAAQS primary standard metric) O_3 in May 2010 are shown in Figures 8a and 8b, and the differences between the F_{SNEI05_ABOTH} and F_{SNEI05_ASUR} cases are shown in Figure 8c (scaled by 5). The updates in California's NO_x emissions (8–13% reductions from the a priori) result in up to 4 ppbv decreases in MDA8 O_3

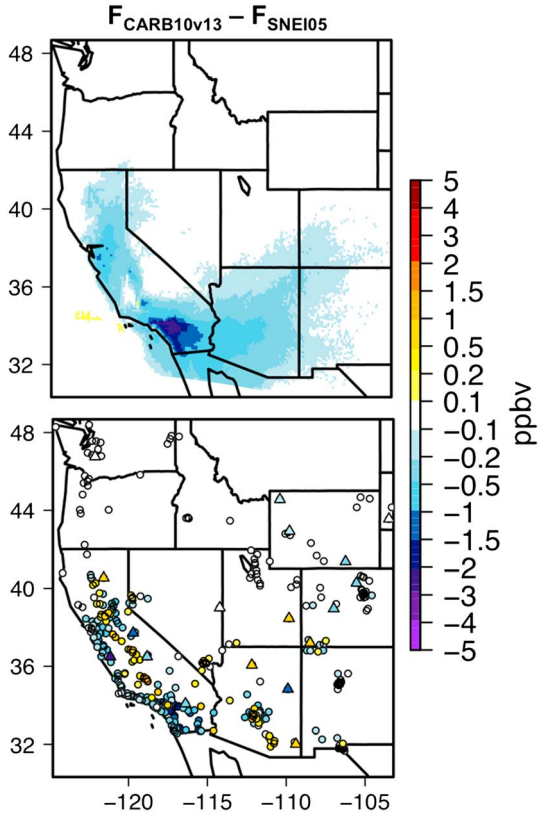

Figure 9. Differences in modeled surface MDA8 O_3 over the Western U.S., between cases $F_{CARB10v13}$ and F_{SNEI05}, scaled by 1/5. (top) The absolute differences, averaged throughout the month. (bottom) The changes in model errors at AQS (circles) and CASTNET (triangles) surface sites, averaged only for the days that observations were available at each site.

from the F_{SNEI05} case in some California regions and the downwind states but an increase in O_3 in few of California's urban areas such as the Greater LA region and the Bay Area by up to 5 ppbv due to the NO_x-saturated chemical regimes that they belong to, as also indicated in our analysis along the WP-3D flight tracks during this month (section 3.2.2) and in previous studies [e.g., *Huang et al.*, 2011; *Chai et al.*, 2013]. Even through the changes in MDA8 O_3 show stronger spatial variability in cases F_{SNEI05_ABOTH} and F_{SNEI05_ASUR} than in F_{SNEI05_ACOL}, we find the similar domain-averaged reductions of 0.2–0.3 ppbv in all three cases. This indicates that the offsetting of regional differences occurred not only in the three sets of a posteriori NO_x emission estimates in California but also in the resulting modeled MDA8 O_3 fields over the Western U.S. Although the a posteriori NO_x emission estimates are also close to $E_{CARB10v13}$ over California, the domain-averaged difference in MDA8 O_3 between $F_{CARB10v13}$ and F_{SNEI05} is significantly larger (~0.5 ppbv, Figure 9) due to the different emissions of non-NO_x O_3 precursors in $E_{CARB10v13}$.

Huang et al. [2013] compared the simulated MDA8 in case F_{SNEI05} with the O_3 measurements at the AQS and CASTNET surface sites and reported a ~5 ppbv mean bias, a ~6 ppbv mean error, and a ~9 ppbv RMSE over the Western U.S. model domain. These uncertainties may be largely attributed to those in the local and regional emission inputs and the model chemistry, as the median profiles of TES and modeled O_3 in this month differ by $<$10% in the free troposphere (Figure 10), which was found dominantly influenced by upper tropospheric air, hemispheric pollution transport, and aged regional pollution during CalNex [*Neuman et al.*, 2012]. The O_3 mean bias at the AQS and CASTNET sites dropped by ~0.5 ppbv (~10%) in the F_{SNEI05_ASUR} and F_{SNEI05_ACOL} cases from case F_{SNEI05}, and case F_{SNEI05_ABOTH} indicates a further reduction in the mean bias of ~0.1 ppbv. The reductions in mean errors and RMSEs in all three a posteriori cases are ~0.3 ppbv (5% and 3% reductions in mean errors and RMSEs, respectively). The errors in modeled O_3 at surface sites were amplified by up to 5 ppbv in a few of California's urban areas in SoCal and the Bay Area but were generally reduced in many rural areas in SoCal and California's downwind states (e.g., Utah, Colorado, Arizona, and New Mexico) ranging from $<$1 to 4 ppbv (Figures 8d and 8e). The spatial patterns of the changes in model error at the surface are qualitatively similar to those along the near-surface flight tracks in California (Figure S4) and are also similar to the differences between cases $F_{CARB10v13}$ and F_{SNEI05} (Figure 9). However, $F_{CARB10v13}$ indicates 0.6–0.7 ppbv lower domain wide mean error, mainly because the more updated non-NO_x emissions in $E_{CARB10v13}$ led to its better performance especially over California's urban regions. In order to further improve the simulated O_3 distributions in top-down studies, additional observational information will need to be integrated to constrain the emissions of non-NO_x species (especially VOCs) in future studies, particularly in the urban areas. Alternatively, assimilating O_3 monitoring data and controlling the initial conditions as in *Chai et al.* [2006, 2007] can directly improve the modeled O_3 fields. Figures 8 and 9 also show that the surface sites in operation then did not cover many regions (e.g., Nevada) where the O_3 distributions changed. Future satellite products, which will have a broader spatial coverage, fine footprint, higher temporal frequency, and higher sensitivity to the boundary layer are expected to improve the evaluation of the modified chemistry fields.

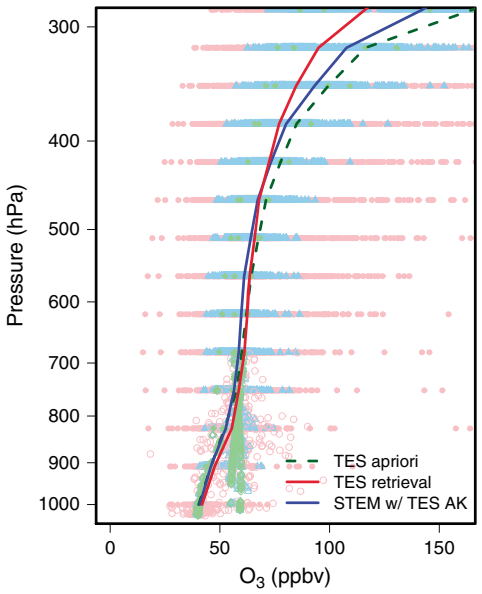

Figure 10. The comparison of O_3 in the F_{SNEI05} case with the TES Level 2 O_3 profiles in the Western U.S. domain in May 2010. Pink, light green, and light blue points denote individual data points from TES retrieval, TES a priori, and STEM modeled O_3, respectively. The filled and unfilled points refer to the data at the TES retrieval pressure levels and at its variable surface pressure levels, respectively. The red, green, and blue solid lines denote the median profiles (calculated only based on data located at the TES retrieval pressure levels) from TES retrieval, TES a priori, and the model, respectively. The model underpredicts the strong variability that TES demonstrates, but the median profiles from TES and model differ by <10%.

Huang et al. [2013] have shown that SoCal anthropogenic pollution (by ~22 million people) can contribute to O_3 in the mountain states in the similar magnitude of those from East Asian (>1.5 billion people) sources estimated by *Lin et al.* [2012] during the CalNex period. They concluded that a relatively small but nearby pollution source can impact a receptor region almost as efficiently as a much larger source that has been diluted over greater transport distances. In this study, we further demonstrated that the impacts of decreasing trend of California's NO_x emissions on O_3 in the mountain states may have compensated those from the Asian pollution associated with an opposite trend [*Cooper et al.*, 2014]. We have also emphasized that improving the estimates of regional anthropogenic emissions (in California and other Pacific states) can help improve the air quality prediction and source contribution analysis of O_3 in the mountain states.

4. Summary and Future Directions

As the observing systems and modeling techniques are being improved, using top-down approaches for timely updates of emission inventories that account for the temporal changes in emissions has become a promising area of research. Such studies help interpret the distributions, trends, and variability of the observed air pollutants. They are expected to also improve the model predictability and assist evaluating the implemented emission control strategies and bottom-up emission projection methodology.

This study explored the capabilities and limitations of assimilating existing space- and ground-based NO_2 observations separately and jointly into the STEM regional chemical transport model at $12 \times 12\ km^2$ horizontal resolution to help quantify the NO_x emission changes in California from 2005 to 2010, using the 4D-Var method. The emission estimates constrained only by NO_2 columns, only by surface NO_2, and by both indicate statewide emission reductions of 26%, 29%, and 30% from 2005 to 2010, respectively. The spatial distributions of the emission changes differed in these cases, which can be attributed to many factors including the differences in the observation sampling strategies and their uncertainties, as well as those in the sensitivities of column and surface NO_2 with respect to NO_x emissions. By comparing with the nonassimilated surface and aircraft measurements, we showed that the modeled NO_2 and O_3 fields in the Western U.S. were overall improved in response to the updates in California's NO_x emissions.

We also examined the consistency of our top-down estimates with several independent inventories. The statewide reductions in NO_x emissions indicated from our observationally constrained emission estimates are also reflected in several independently developed inventories: ~30% in the CARB bottom-up inventory, ~4% in the 2008 National Emission Inventory, and ~20% in the annual mean top-down estimates by Lamsal et al. (Figure S1) using the global GEOS-Chem model and OMI NO_2 columns. Despite the grid-scale differences among all top-down and bottom-up inventories, they all indicate stronger emission reductions in the urban regions. Interpretation of the discrepancies among various NO_x inventories on grid scale, as well as improving the estimates of other O_3 precursors' emissions, can benefit future air quality modeling and policy decision.

These "top-down" approaches in future studies may be improved in the aspects of assimilated observations, the used model, and the assimilation setup. U.S. EPA has set high priority for evaluating the catalytic

conversion/CL-detection method (the Federal Reference Method since the 1970s) to monitor surface NO_2, including its comparison with the photolytic conversion/CL detection method that has recently been defined as Federal Equivalent Method [*Hall et al*., 2012]. A geostationary satellite TEMPO over the North America will be launched in 2018–2019 [*Chance et al*., 2013]. Alternative terrain pressure, albedo, and NO_2 a priori profiles have been used in vertical column NO_2 retrievals [*Russell et al*., 2011], which provided useful information for quantifying and reducing biases in the current retrievals. Therefore, in the near future, it will be possible to use space- and ground-based monitoring data of multiple species associated with lower uncertainties that are sampled more broadly and frequently. Recent field campaigns (e.g., DISCOVER-AQ and SEAC^{4}RS) that provided vertical profiles of multiple chemical species under various weather conditions can advance our understanding of the relationships between surface and column observations. They may also benefit the AMF calculations and the effectiveness of data assimilation. Great efforts should be made to keep improving the model meteorology, chemistry, and deposition that affect the assimilation results. More experiments should be conducted to improve the configurations of the assimilation, such as careful selections of control variables and assimilation windows, and better estimates of errors. Developing the assimilation of slant column retrievals will need to be considered to avoid the impact of uncertainties in vertical column retrievals introduced from the AMFs and the AKs (as discussed in section 2.1.1).

This work is a critical step toward advancing our understanding of the changes in emissions and distributions of air pollutants. It also shows the potential of using space-/ground-based monitoring data and advanced data assimilation approach to timely and independently update NO_x emission estimates on a monthly scale and at a fine grid resolution. The well-evaluated results here suggest that these approaches can be applied more broadly.

Acknowledgments

This work was initiated at the University of Iowa and supported by a NASA award NNX11AI52G. It was continued at Jet Propulsion Laboratory, California Institute of Technology, under a contract with NASA, supported by the NASA Aura project. We thank the CalNex and Aura science teams, and the open access to the used observation data and the NO_x emission scaling factors created by Lamsal et al. The sources of data are cited in text and Table 1. We also acknowledge the computational resources at the University of Iowa and at NASA Ames Research Center. The views, opinions, and findings contained in this paper are those of the authors and should not be construed as an official NOAA or U.S. Government position, policy, or decision.

References

Adhikary, B., et al. (2010), A regional scale modeling analysis of aerosol and trace gas distributions over the eastern Pacific during the INTEX-B field campaign, *Atmos. Chem. Phys.*, *10*, 2091–2115.

Akima, H. (1970), A new method of interpolation and smooth curve fitting based on local procedures, *J. ACM*, *17*, 589–602.

Bechle, M. J., D. B. Millet, and J. D. Marshall (2013), Remote sensing of exposure to NO_2: Satellite versus ground-based measurement in a large urban area, *Atmos. Environ.*, *69*, 345–353.

Beer, R. (2006), TES on the Aura mission: Scientific objectives, measurements, and analysis overview, *IEEE Trans. Geosci. Remote Sens.*, *44*, 1102–1105.

Beirle, S., K. F. Boersma, U. Platt, M. G. Lawrence, and T. Wagner (2011), Megacity emissions and lifetimes of nitrogen oxides probed from space, *Science*, *333*, 1737–1739.

Boersma, K. F., et al. (2007), Near-real time retrieval of tropospheric NO_2 from OMI, *Atmos. Chem. Phys.*, *7*, 2013–2128.

Boersma, K. F., et al. (2008), Validation of OMI tropospheric NO_2 observations during INTEX-B and application to constrain NOx emissions over the eastern United States and Mexico, *Atmos. Environ.*, *42*, 4480–4497.

Boersma, K. F., D. J. Jacob, M. Trainic, Y. Rudich, I. DeSmedt, R. Dirksen, and H. J. Eskes (2009), Validation of urban NO_2 concentrations and their diurnal and seasonal variations observed from the SCIAMACHY and OMI sensors using in situ surface measurements in Israeli cities, *Atmos. Chem. Phys.*, *9*, 3867–3879.

Boersma, K. F., R. Braak, and R. J. van der A (2011a), Dutch OMI NO_2 (DOMINO) data product v2.0 HE5 data file user manual. [Available at http://www.temis.nl/docs/OMI_NO2_HE5_2.0_2011.pdf.]

Boersma, K. F., et al. (2011b), An improved tropospheric NO_2 column retrieval algorithm for the Ozone Monitoring Instrument, *Atmos. Meas. Tech.*, *4*, 1905–1928.

Bowman, K., and D. K. Henze (2012), Attribution of direct ozone radiative forcing to spatially resolved emissions, *Geophys. Res. Lett.*, *39*, L22704, doi:10.1029/2012GL053274.

Bowman, K. W., et al. (2006), Tropospheric emission spectrometer: Retrieval method and error analysis, *IEEE Trans. Geosci. Remote Sens.*, *44*, 1297–1307.

Boxe, C. S., et al. (2010), Validation of northern latitude Tropospheric Emission Spectrometer stare ozone profiles with ARC-IONS sondes during ARCTAS: Sensitivity, bias and error analysis, *Atmos. Chem. Phys.*, *10*, 9901–9914.

Brioude, J., et al. (2013), Top-down estimate of surface flux in the Los Angeles Basin using a mesoscale inverse modeling technique: Assessing anthropogenic emissions of CO, NO_x and CO_2 and their impacts, *Atmos. Chem. Phys.*, *13*, 3661–3677.

Burley, J. D., A. Bytnerowicz, J. D. Ray, S. Schilling, and E. B. Allen (2014), Surface ozone in Joshua Tree National Park, *Atmos. Environ.*, *87*, 95–107.

California Air Resources Board (CARB) (2014), 2013 California almanac of emissions and air quality. [Available at http://www.arb.ca.gov/aqd/almanac/almanac13/almanac2013all.pdf.]

Carmichael, G. R., et al. (2003a), Evaluating regional emission estimates using the TRACE-P observations, *J. Geophys. Res.*, *108*(D21), 8810, doi:10.1029/2002JD003116.

Carmichael, G. R., et al. (2003b), Regional-scale chemical transport modeling in support of the analysis of observations obtained during the TRACE-P experiment, *J. Geophys. Res.*, *108*(D21), 8823, doi:10.1029/2002JD003117.

Carmichael, G. R., A. Sandu, T. Chai, D. N. Daescu, E. M. Constantinescu, and Y. Tang (2008), Predicting air quality: Improvements through advanced methods to integrate models and measurements, *J. Comput. Phys.*, *227*, 3540–3571.

Carter, W. P. L. (2000), Documentation of the SAPRC-99 chemical mechanism for VOC Reactivity Assessment, final report to California Air Resources Board, Contract No. 92–329 and 95–308.

CASTNET (2011), Clean air status and trends network 2011 annual report. [Available at http://epa.gov/castnet/javaweb/docs/annual_report_201.pdf.]

Chai, T., G. R. Carmichael, A. Sandu, Y. Tang, and D. N. Daescu (2006), Chemical data assimilation of Transport and Chemical Evolution over the Pacific (TRACE-P) aircraft measurements, *J. Geophys. Res.*, *111*, D02301, doi:10.1029/2005JD005883.

Chai, T., et al. (2007), Four dimensional data assimilation experiments with International Consortium for Atmospheric Research on Transport and Transformation ozone measurements, *J. Geophys. Res.*, *112*, D12S15, doi:10.1029/2006JD007763.

Chai, T., G. R. Carmichael, Y. Tang, A. Sandu, A. Heckel, A. Richter, and J. P. Burrows (2009), Regional NO_x emission inversion through a four-dimensional variational approach using SCIAMACHY tropospheric NO_2 column observations, *Atmos. Environ.*, *43*, 5046–5055.

Chai, T., H.-C. Kim, P. Lee, D. Tong, L. Pan, Y. Tang, J. Huang, J. McQueen, M. Tsidulko, and I. Stajner (2013), Evaluation of the United States National Air Quality Forecast Capability experimental real-time predictions in 2010 using Air Quality System ozone and NO_2 measurements, *Geosci. Model Dev.*, *6*, 1831–1850.

Chance, K., X. Liu, D. E. Flittner, J. Al-Saadi, and S. J. Janz (2013), Tropospheric emissions: Monitoring of pollution (TEMPO). [Available at http://www.cfa.harvard.edu/atmosphere/publications/TEMPO-SPIE-2013-24aug2013.pdf.]

Colman, J. J., A. L. Swanson, S. Meinardi, B. C. Sive, D. R. Blake, and F. S. Rowland (2011), Description of the analysis of a wide range of volatile organic compounds in whole air samples collected during PEM-Tropics A and B, *Anal. Chem.*, *73*, 3723–3731.

Cooper, O. R., et al. (2014), Global distribution and trends of tropospheric ozone: An observation-based review, *Elem. Sci. Anth.*, *2*, doi:10.12952/journal.elementa.000029.

Duncan, B., et al. (2010), Application of OMI observations to a space-based indicator of NO_x and VOC controls on surface ozone formation, *Atmos. Environ.*, *44*, 2213–2223.

Duncan, B., et al. (2014), Quantifying uncertainties of OMI NO_2 data: Implications for air quality applications. [Available at http://acmg.seas.harvard.edu/aqast/meetings/2014_jan/program.html.]

Dunlea, E. J., et al. (2007), Evaluation of nitrogen dioxide chemiluminescence monitors in a polluted urban environment, *Atmos. Chem. Phys.*, *7*, 2691–2704.

Eskes, H. J., and K. F. Boersma (2003), Averaging kernels for DOAS total-column satellite retrievals, *Atmos. Chem. Phys.*, *3*, 1285–1291.

Eskes, H. J., P. F. J. Velthoven, P. J. M. Valks, and H. M. Kelder (2003), Assimilation of GOME total-ozone satellite observations in a three-dimensional tracer-transport model, *Q. J. R. Meteorol. Soc.*, *129*, 1663–1681.

Fishman, J., M. L. Silverman, J. H. Crawford, and J. K. Creilson (2011), A study of regional-scale variability of in situ and model-generated tropospheric trace gases: Insights into observational requirements for a satellite in geostationary orbit, *Atmos. Environ.*, *45*, 4682–4694.

Fishman, J., et al. (2012), The United State' Next Generation of Atmospheric Composition and Coastal Ecosystem Measurements: NASA's Geostationary Coastal and Air Pollution Events (GEO-CAPE) Mission, *Bull. Am. Meteorol. Soc.*, *93*, 1547–1566.

Hakami, A., D. K. Henze, J. H. Seinfeld, T. Chai, Y. Tang, G. R. Carmichael, and A. Sandu (2005), Adjoint inverse modeling of black carbon during the Asian Pacific Regional Aerosol Characterization Experiment, *J. Geophys. Res.*, *110*, D14301, doi:10.1029/2004JD005671.

Hakami, A., J. H. Seinfeld, T. F. Chai, Y. H. Tang, G. R. Carmichael, and A. Sandu (2006), Adjoint sensitivity analysis of ozone nonattainment over the continental United States, *Environ. Sci. Technol.*, *40*, 3855–3864.

Hall, E., M. Beaver, R. W. Long, and R. W. Vanderpool (2012), EPA's reference and equivalent supporting NAAQS implementation through methods research program: Research, development, and analysis, *Air Waste Manage. Assoc. Mag. Environ. Managers*, *5*, 8–12.

Heckel, A., S.-W. Kim, G. J. Frost, A. Richter, M. Trainer, and J. P. Burrows (2011), Influence of low spatial resolution a priori data on tropospheric NO_2 satellite retrievals, *Atmos. Meas. Tech.*, *4*, 1805–1820.

Herron-Thorpe, F. L., B. K. Lamb, G. H. Mount, and J. K. Vaughan (2010), Evaluation of a regional air quality forecast model for tropospheric NO_2 columns using the OMI/Aura satellite tropospheric NO_2 product, *Atmos. Chem. Phys.*, *10*, 8839–8854.

Huang, M., et al. (2010), Impacts of transported background ozone on California air quality during the ARCTAS-CARB period—A multi-scale modeling study, *Atmos. Chem. Phys.*, *10*, 6947–6968.

Huang, M., et al. (2011), Multi-scale modeling study of the source contributions to near-surface ozone and sulfur oxides levels over California during the ARCTAS-CARB period, *Atmos. Chem. Phys.*, *11*, 3173–3194.

Huang, M., K. W. Bowman, G. R. Carmichael, R. B. Pierce, H. M. Worden, M. Luo, O. R. Cooper, I. B. Pollack, T. B. Ryerson, and S. S. Brown (2013), Impact of southern California anthropogenic emissions on ozone pollution in the mountain states: Model analysis and observational evidence from space, *J. Geophys. Res. Atmos.*, *118*, 12,784–12,803, doi:10.1002/2013JD020205.

Kopacz, M., D. L. Mauzerall, J. Wang, E. M. Leibensperger, D. K. Henze, and K. Singh (2011), Origin and radiative forcing of black carbon transported to the Himalayas and Tibetan Plateau, *Atmos. Chem. Phys.*, *11*, 2837–2852.

Lamsal, L. N., R. V. Martin, A. van Donkelaar, M. Steinbacher, E. A. Celarier, E. Bucsela, and E. J. Dunlea, J. P. Pinto (2008), Ground-level nitrogen dioxide concentrations inferred from the satellite-borne Ozone Monitoring Instrument, *J. Geophys. Res.*, *113*, D16308, doi:10.1029/2007JD009235.

Lamsal, L. N., R. V. Martin, A. van Donkelaar, E. A. Celarier, E. J. Bucsela, K. F. Boersma, R. Dirksen, C. Luo, and Y. Wang (2010), Indirect validation of tropospheric nitrogen dioxide retrieved from the OMI satellite instrument: Insight into the seasonal variation of nitrogen oxides at northern midlatitudes, *J. Geophys. Res.*, *115*, D05302, doi:10.1029/2009JD013351.

Lamsal, L. N., R. V. Martin, A. Padmanabhan, A. van Donkelaar, Q. Zhang, C. E. Sioris, K. Chance, T. P. Kurosu, and M. J. Newchurch (2011), Application of satellite observations for timely updates to global anthropogenic NO_x emission inventories, *Geophys. Res. Lett.*, *38*, L05810, doi:10.1029/2010GL046476.

Lamsal, L. N., R. V. Martin, D. D. Parrish, and N. A. Krotkov (2013), Scaling relationship for NO_2 pollution and urban population size: A satellite perspective, *Environ. Sci. Technol.*, *47*, 7855–7861.

Langford, A. O., C. J. Senff, R. J. Alvarez II, R. M. Banta, and R. M. Hardesty (2010), Long-range transport of ozone from the Los Angeles Basin: A case study. *Geophys. Res. Lett.*, *37*, L06807, doi:10.1029/2010GL042507.

Lapina, K., D. K. Henze, J. B. Milford, M. Huang, M. Lin, A. M. Fiore, G. Carmichael, G. G. Pfister, and K. Bowman (2014), Assessment of source contributions to seasonal vegetative exposure to ozone in the U.S., *J. Geophys. Res. Atmos.*, *119*, 324–340, doi:10.1002/2013JD020905.

Lauvaux, T., and K. J. Davis (2014), Planetary boundary layer errors in mesoscale inversions of column-integrated CO_2 measurements, *J. Geophys. Res. Atmos.*, *119*, 490–508, doi:10.1002/2013JD020175.

Levelt, P. F., G. H. J. van den Oord, M. R. Dobber, A. Malkki, H. Visser, J. de Vries, P. Stammes, J. O. V. Lundell, and H. Saari (2006), The Ozone Monitoring Instrument, *IEEE Trans. Geosci. Remote Sens.*, *44*(5), 1093–1101, doi:10.1109/TGRS.2006.872333.

Lin, M., et al. (2012), Transport of Asian ozone pollution into surface air over the western United States in spring, *J. Geophys. Res.*, *117*, D00V07, doi:10.1029/2011JD016961.

Madronich, S., S. Flocke, J. Zeng, I. Petropavlovskikh, and J. Lee-Taylor (2002), The Tropospheric Ultra-violet Visible (TUV) model Manual. [Available at http://www.acd.ucar.edu/.]

Martin, R. V., D. J. Jacob, K. V. Chance, T. P. Kurosu, P. I. Palmer, and M. J. Evans (2003), Global inventory of nitrogen oxide emissions constrained by space-based observations of NO_2 columns, *J. Geophys. Res.*, *108*(D17), 4537, doi:10.1029/2003JD003453.

McCarthy, J. E. (2010), Ozone air quality standards: EPA's proposed January 2010 revision. [Available at http://www.fas.org/sgp/crs/misc/R41062.pdf.]
McDonald, B. C., T. R. Dallmann, E. W. Martin, and R. A. Harley (2012), Long-term trends in nitrogen oxide emissions from motor vehicles at national, state, and air basin scales, *J. Geophys. Res.*, *117*, D00V18, doi:10.1029/2012JD018304.
McLinden, C. A., Fioletov, V., Boersma, K. F., Krotkov, N., Sioris, C. E., Veefkind, J. P., Yang, K. (2012), Air quality over the Canadian oil sands: A first assessment using satellite observations. *Geophys. Res. Lett.*, *39*, L04804, doi:10.1029/2011GL050273.
McPeters, R., M. Kroon, G. Labow, E. Brinksma, D. Balis, I. Petropavlovskikh, J. P. Veefkind, P. K. Bhartia, and P. F. Levelt (2008), Validation of the Aura Ozone Monitoring Instrument total column ozone product, *J. Geophys. Res.*, *113*, D15S14, doi:10.1029/2007JD008802.
Miyazaki, K., H. J. Eskes, and K. Sudo (2012a), Global NO_x emission estimates derived from an assimilation of OMI tropospheric NO_2 columns, *Atmos. Chem. Phys.*, *12*, 2263–2288.
Miyazaki, K., H. J. Eskes, K. Sudo, M. Takigawa, M. van Weele, and K. F. Boersma (2012b), Simultaneous assimilation of satellite NO_2, O_3, CO, and HNO_3 data for the analysis of tropospheric chemical composition and emissions, *Atmos. Chem. Phys.*, *12*, 9545–9579.
Nassar, R., et al. (2008), Validation of Tropospheric Emission Spectrometer (TES) nadir ozone profiles using ozonesonde measurements, *J. Geophys. Res.*, *113*, D15S17, doi:10.1029/2007JD008819.
Neuman, J. A., L. G. Huey, T. B. Ryerson, and D. W. Fahey (1999), Study of inlet materials for sampling atmospheric nitric acid, *Environ. Sci. Technol.*, *33*, 1133–1136.
Neuman, J. A., et al. (2002), Fast-response airborne in situ measurements of HNO_3 during the Texas 2000 Air Quality Study. *J. Geophys. Res.*, *107*(D20), 4436, doi:10.1029/2001JD001437.
Neuman, J. A., et al. (2012), Observations of ozone transport from the free troposphere to the Los Angeles basin, *J. Geophys. Res.*, *117*, D00V09, doi:10.1029/2011JD016919.
Office of Air Quality Planning and Standards (2008), Quality assurance handbook for air pollution measurement systems, vol. II: Ambient air quality monitoring program. [Available at http://www.epa.gov/ttn/amtic/files/ambient/pm25/qa/QA-Handbook-Vol-II.pdf.]
Palmer, P. I., D. J. Jacob, K. Chance, R. V. Martin, R. J. D. Spurr, T. P. Kurosu, I. Bey, R. Yantosca, A. Fiore, and Q. Li (2001), Air mass factor formulation for spectroscopic measurements from satellites: Application to formaldehyde retrievals from the Global Ozone Monitoring Experiment, *J. Geophys. Res.*, *106*, 14,539–14,550, doi:10.1029/2000JD900772.
Pfister, G., S. Walters, L. K. Emmons, and D. P. Edwards (2013), Quantifying the contribution of inflow on surface ozone over California, *J. Geophys. Res. Atmos.*, *118*, 12,282–12,299, doi:10.1002/2013JD020336.
Pierce, R. B., et al. (2007), Chemical data assimilation estimates of continental U.S. ozone and nitrogen budgets during the Intercontinental Chemical Transport Experiment–North America, *J. Geophys. Res.*, *112*, D12S21, doi:10.1029/2006JD007722.
Pierce, R. B., et al. (2011), Chemical and aerosol data assimilation activities during CalNex. [Available at http://www.arb.ca.gov/research/calnex2010/da_workshop_may2011/tuesday/calnex_data_workshop_pierce_final.pdf.]
Pollack, I. B., B. M. Lerner, and T. B. Ryerson (2011), Evaluation of ultraviolet light-emitting diodes for detection of atmospheric NO_2 by photolysis-chemiluminescence, *J. Atmos. Chem.*, *65*, 111–125.
Pollack, I. B., T. B. Ryerson, M. Trainer, J. A. Neuman, J. M. Roberts, and D. D. Parrish (2013), Trends in ozone, its precursors, and related secondary oxidation products in Los Angeles, California: A synthesis of measurements from 1960 to 2010, *J. Geophys. Res. Atmos.*, *118*, 5893–5911, doi:10.1002/jgrd.50472.
Pusede, S. E., and R. C. Cohen (2012), On the observed response of ozone to NO_x and VOC reactivity reductions in San Joaquin Valley California 1995–present, *Atmos. Chem. Phys.*, *12*, 8323–8339.
Richards, N. A. D., G. B. Osterman, E. V. Browell, J. W. Hair, M. Avery, and Q. Li (2008), Validation of Tropospheric Emission Spectrometer ozone profiles with aircraft observations during the Intercontinental Chemical Transport Experiment–B, *J. Geophys. Res.*, *113*, D16S29, doi:10.1029/2007JD008815.
Roiger, A., H. Aufmhoff, P. Stock, F. Arnold, and H. Schlager (2011), An aircraft-borne chemical ionization–ion trap mass spectrometer (CI-ITMS) for fast PAN and PPN measurements, *Atmos. Meas. Tech.*, *4*, 173–188.
Russell, A. R., L. C. Valin, E. J. Buscela, M. O. Wenig, and R. C. Cohen (2010), Space-based constraints on spatial and temporal patterns of NO_x emissions in California 2005–2008, *Environ. Sci. Technol.*, *44*, 3608–3615.
Russell, A. R., A. E. Perring, L. C. Valin, R. C. Hudman, E. C. Browne, K.-E. Min, P. J. Wooldridge, and R. C. Cohen (2011), A high spatial resolution retrieval of NO_2 column densities from OMI: Method and evaluation, *Atmos. Chem. Phys.*, *11*, 8543–8554.
Russell, A. R., L. C. Valin, and R. C. Cohen (2012), Trends in OMI NO_2 observations over the United States: Effects of emission control technology and the economic recession, *Atmos. Chem. Phys.*, *12*, 12,197–12,209.
Ryerson, T. B., et al. (1998), Emissions lifetimes and ozone formation in power plant plumes, *J. Geophys. Res.*, *103*, 22,569–22,583, doi:10.1029/98JD01620.
Ryerson, T. B., et al. (2013), The 2010 California Research at the Nexus of Air Quality and Climate Change (CalNex) field study, *J. Geophys. Res. Atmos.*, *118*, 5830–5866, doi:10.1002/jgrd.50331.
Sandu, A., D. N. Daescu, G. R. Carmichael, and T. Chai (2005), Adjoint sensitivity analysis of regional air quality models, *J. Comput. Phys.*, *204*, 222–252.
Silver, J. D., J. Brandt, M. Hvidberg, J. Frydendall, and J. H. Christensen (2013), Assimilation of OMI NO_2 retrievals into the limited-area chemistry-transport model DEHM (V2009.0) with a 3-D OI algorithm, *Geosci. Model Dev.*, *6*, 1–16.
Skamarock, W. C., J. B. Klemp, J. Dudhia, D. Gill, D. M. Barker, W. Wang, and J. G. Powers (2008), A description of the advanced research WRF version 3. [Available at: www.mmm.ucar.edu/wrf/users/docs/arwv3.pdfv3.pdf.]
Steinbacher, M., C. Zellweger, B. Schwarzenbach, S. Bugmann, B. Buchmann, C. Ordóñez, A. S. H. Prevot, and C. Hueglin (2007), Nitrogen oxide measurements at rural sites in Switzerland: Bias of conventional measurement techniques, *J. Geophys. Res.*, *112*, D11307, doi:10.1029/2006JD007971.
Stewart, L. M., S. L. Dance, and N. K. Nichols (2008), Correlated observation errors in data assimilation, *Int. J. Numer. Meth. Fluid.*, *56*, 1521–1527.
Stewart, L. M., S. Dance, and N. K. Nichols (2013), Data assimilation with correlated observation errors: Experiments with a 1-D shallow water model, *Tellus A*, *65*, 19546.
Stith, J. L., et al. (2009), An overview of aircraft observations from the Pacific dust experiment campaign, *J. Geophys. Res.*, *114*, D05207, doi:10.1029/2008JD010924.
Tang, W., D. S. Cohan, L. N. Lamsal, X. Xiao, and W. Zhou (2013), Inverse modeling of Texas NO_x emissions using space-based and ground-based NO_2 observations, *Atmos. Chem. Phys.*, *13*, 11,005–11,018.
Tang, Y., et al. (2004), Multiscale simulations of tropospheric chemistry in the eastern Pacific and on the U. S. West Coast during spring 2002, *J. Geophys. Res.*, *109*, D23S11, doi:10.1029/2004JD004513.
Tang, Y. H., et al. (2007), Influence of lateral and top boundary conditions on regional air quality prediction: A multiscale study coupling regional and global chemical transport models, *J. Geophys. Res.*, *112*, D10S18, doi:10.1029/2006JD007515.

Tong, D. Q., and D. L. Mauzerall (2008), Summertime state-level source-receptor relationships between nitrogen oxide emissions and downwind surface ozone concentrations over the Continental United States, *Environ. Sci. Technol.*, *42*, 7976–7984.

Turner, A., D. K. Henze, R. V. Martin, and A. Hakami (2012), The spatial extent of source influences on modeled column concentrations of short-lived species, *Geophys. Res. Lett.*, *39*, L12806, doi:10.1029/2012GL051832.

U.S. Census Bureau 2010 (2011), Available at http://factfinder2.census.gov/faces/nav/jsf/pages/index.xhtml.

U.S. Environmental Protection Agency (EPA) (2010), Fact sheet: Proposal to revise the national ambient air quality standards for ozone. [Available at http://www.epa.gov/air/ozonepollution/pdfs/fs20100106std.pdf.]

U.S. Environmental Protection Agency (EPA) (2013), Integrated science assessment for oxides of nitrogen-health criteria. [Available at http://cfpub.epa.gov/ncea/isa/recordisplay.cfm?deid=259167.]

U.S. Environmental Protection Agency (EPA) (2014), Policy assessment for the review of the ozone National Ambient Air Quality Standards, 2nd external review draft. [Available at http://www.epa.gov/ttn/naaqs/standards/ozone/data/20140131pa.pdf.]

Valin, L. C., A. R. Russell, R. C. Hudman, and R. C. Cohen (2011), Effects of model resolution on the interpretation of satellite NO_2 observations, *Atmos. Chem. Phys.*, *11*, 11,647–11,655.

Valin, L. C., A. R. Russell, and R. C. Cohen (2013), Variations of OH radical in an urban plume inferred from NO_2 column measurements, *Geophys. Res. Lett.*, *40*, 1856–1860, doi:10.1002/grl.50267.

Valin, L. C., A. R. Russell, and R. C. Cohen (2014), Chemical feedback effects on the spatial patterns of the NO_x weekend effect: A sensitivity analysis, *Atmos. Chem. Phys.*, *14*, 1–9.

VanCuren, R. (2014), Transport aloft drives peak ozone in the Mojave Desert, *Atmos. Environ.*, doi:10.1016/j.atmosenv.2014.09.057.

Verstraeten, W. W., K. F. Boersma, J. Zörner, M. A. F. Allaart, K. W. Bowman, and J. R. Worden (2013), Validation of six years of TES tropospheric ozone retrievals with ozonesonde measurements: Implications for spatial patterns and temporal stability in the bias, *Atmos. Meas. Tech.*, *6*, 1413–1423.

Warneke, C., J. A. de Gouw, J. S. Holloway, J. Peischl, T. B. Ryerson, E. Atlas, D. Blake, M. Trainer, and D. D. Parrish (2012), Multiyear trends in volatile organic compounds in Los Angeles, California: Five decades of decreasing emissions, *J. Geophys. Res.*, *117*, D00V17, doi:10.1029/2012JD017899.

Winer, A. M., J. W. Peters, J. P. Smith, and J. N. Pitts (1974), Response of commercial chemiluminescent nitric oxide-nitrogen dioxide analyzers to other nitrogen-containing compounds, *Environ. Sci. Technol.*, *8*(13), 1118–1121.

Witte, J., B. Duncan, A. Douglass, T. Kurosu, K. Chance, and C. Retscher (2011), The unique OMI $HCHO/NO_2$ feature during the 2008 Beijing Summer Olympics: Implications for ozone production sensitivity, *Atmos. Environ.*, *45*, 3103–3111.

Xing, J., J. Pleim, R. Mathur, G. Pouliot, C. Hogrefe, C.-M. Gan, and C. Wei (2013), Historical gaseous and primary aerosol emissions in the United States from 1990 to 2010, *Atmos. Chem. Phys.*, *13*, 7531–7549.

Zhang, L., D. J. Jacob, M. Kopacz, D. K. Henze, K. Singh, and D. A. Jaffe (2009), Intercontinental source attribution of ozone pollution at western U.S. sites using an adjoint method, *Geophys. Res. Lett.*, *36*, L11810, doi:10.1029/2009GL037950.

Zhang, Y., Y. Chen, G. Sarwar, and K. Schere (2012), Impact of gas-phase mechanisms on Weather Research Forecasting Model with Chemistry (WRF/Chem) predictions: Mechanism implementation and comparative evaluation, *J. Geophys. Res.*, *117*, D01301, doi:10.1029/2011JD015775.

Zhu, C., R. H. Byrd, P. Lu, and J. Nocedal (1997), L-BFGS-B--fortran routines for large scale bound constrained optimization, *ACM Trans. Math. Softw.*, *23*, 550–560.

Zoogman, P., D. J. Jacob, K. Chance, L. Zhang, P. Le Sager, A. M. Fiore, A. Eldering, X. Liu, V. Natraj, and S. S. Kulawik (2011), Ozone air quality measurement requirements for a geostationary satellite mission, *Atmos. Environ.*, *45*, 7143–7150.